January 2015

Effect of Strontium in Soldering Resistance

Pengyu Zhu
Purdue University

Graduate School Form 30
Updated 1/15/2015

PURDUE UNIVERSITY
GRADUATE SCHOOL
Thesis/Dissertation Acceptance

This is to certify that the thesis/dissertation prepared

By Pengyu Zhu

Entitled

EFFECT OF STRONTIUM IN SOLDERING RESISTANCE

For the degree of Master of Science

Is approved by the final examining committee:

Qingyou Han
Chair

Xiaoming Wang

Milan Rakita

To the best of my knowledge and as understood by the student in the Thesis/Dissertation Agreement, Publication Delay, and Certification Disclaimer (Graduate School Form 32), this thesis/dissertation adheres to the provisions of Purdue University's "Policy of Integrity in Research" and the use of copyright material.

Approved by Major Professor(s): Qingyou Han

Approved by: Kathy Newton 12/2/2015

Head of the Departmental Graduate Program Date

EFFECT OF STRONTIUM IN SOLDERING RESISTANCE

A Thesis

Submitted to the Faculty

of

Purdue University

by

Pengyu Zhu

In Partial Fulfillment of the

Requirements for the Degree

of

Master of Science

December 2015

Purdue University

West Lafayette, Indiana

ACKNOWLEDGEMENTS

Firstly, I would like to thank my advisor Dr. Qingyou Han. He has provided me an opportunity to study at this world-renowned university, Purdue. I couldn't have received my master's degree without his help both in academics and finances. His unconditional support, encouragement, unlimited patience, guidance and enthusiasm supported me completely during my research. He made my two years study become my life wealth. His kindness offered me more space to express my childish ideas and his wisdom will illuminate my future life.

Secondly, I am also very grateful to my committee members, Dr. Milan Rakita and Dr. Xiaoming Wang. I am also very grateful to Dr. Duane D Dunlap for helping me edit my thesis. Special thanks to Prof. Kmec for helping revise the thesis.

I really appreciate the support from Dr. Wilson Xu and Dr. Xiaoming Wang. Working with them has been a very pleasant experience.

I am thankful also very thankful for all those following people in my research group, including Juncheng Zhu, Dr Zhiwei Liu, Dr Meng Wang, Wei Dai, Fei He, Fei Yin, Pu Wang, Yanfei Liu, Ian McAdams and Xingtao Liu. I enjoy the time with you.

Finally, I want to acknowledge my parents and all other family members. This dissertation would not have been finished without their selfless support.

TABLE OF CONTENTS

Page
LIST OF TABLES v
LIST OF FIGURES vi
LIST OF ABBREVIATIONS viii
GLOSSARY ix
ABSTRACT x
CHAPTER 1 INTRODUCTION 1
1.1 Scope 2
1.2 Significance of This Research 3
1.3 Research Questions 6
1.4 Assumptions 6
1.5 Limitations 7
1.6 Delimitations 7
1.7 Summary 7
CHAPTER 2 LITERATURE REVIEW 8
2.1 Outline 8
2.2 Die Soldering 8
2.2.1 Die Soldering Introduction and BackGround 9
2.2.2 Die Soldering Introduction 10
2.2.3 Critical Temperature for Soldering Reaction 12
2.3 Properties of A380 Aluminum Alloy 15
2.3.1 Al-Si System 15
2.3.2 Morphology and Properties of α-phase and β-phase 17
2.3.3 Si-Sr Diagram 18
2.3.4 Al-Si-Sr Intermetallic 19
2.4 Segregation behavior of Strontium 21
2.5 Strontium Effect 25
2.6 Summary 28
CHAPTER 3 METHODOLOGY 29
3.1 Sample Approach 30
3.2 Research Hypothesis 33
3.3 Data Collection 34
3.3.1 Measuring the Proportion of Strontium 34
3.3.2 Solidification Simulation 34
3.3.3 Second Dendrite Arm Spacing 38
3.4 Instrumentation 39

Page

3.5 Data Analysis 42
3.6 Standard of Success 42
3.7 Summary 43
CHAPTER 4 EXPERIMENTAL RESULTS 44
4.1 Determine Solidifying Direction 44
4.2 Eutectic Structure 47
4.3 Strontium Distribution 52
4.3.1 Composition of Diamond-Shaped Particles 52
4.3.2 Cross Section of Soldering Area 56
4.3.3 Detection of Strontium Oxide Layer on Soldering Areas 58
4.4 Summary 62
CHAPTER 5 CONCLUSIONS AND FUTURE WORK 63
5.1 Discussion 63
5.1.1 Discuss of Strontium Particles on Nucleation 63
5.1.2 Discussion of Formation of Strontium Oxide 64
5.2 Conclusions 65
5.3 Future Work 66
LIST OF REFERENCES 68
APPENDIX 72
VITA 74

LIST OF TABLES

Table Page
Table 1.1 New Proposed alloys. 4
Table 2.1 Al-Si-Sr ternary Intermetallic. 20
Table 2.2 Composition of Mercalloy. 26
Table 3.1 A380 Components. 30
Table 3.2 Compositions and Pouring Temperature. 33
Table 3.3 Composition of Solution for Electro-Polishing. 40
Table 4.1 Second Dendrite Arm Spaces in Different Specimens. 47
Table 4.2 Quantitative Data of Composition. 54
Table 4.3 Al-Si-Sr ternary Intermetallic. 55
Table 4.4 Compositions of Selected Particles..... 57
Table 4.5 Global Composition of Cross Section Area..... 57
Table 4.6 Quantitative Composition of Selected Spots At%. 60
Table 4.7 Quantitative Composition of Selected Spots At%. 62

LIST OF FIGURES

Figure Page
Figure 1.1 Die Soldering on Core Pin 2
Figure 2.1 Intermetallic Layers of Soldering on H13 Steel Die 10
Figure 2.2 Schematic Process of the Formation of Intermetallic Layers 11
Figure 2.3 Al-Fe Phase Diagram 13
Figure 2.4 Schematic illustration showing possible aluminum composition and temperature profiles at the die surface 14
Figure 2.5 Al-Si Equilibrium phase diagram 16
Figure 2.6 Interleaved Structures 17
Figure 2.7 Si-Sr Phase Diagram 18
Figure 2.8 Solidification Zones 21
Figure 2.9 Al-Sr Equilibrium phase diagram 23
Figure 2.10 Component Diffusion Process 24
Figure 2.11 Porosity Modified by Strontium 27
Figure 3.1 STesting Cylindrical Steel Bar 29
Figure 3.2 Permanent Mold 31
Figure 3.3 Experiment Set 32
Figure 3.4 Sample Approach 32
Figure 3.5 Flow Pattern 36
Figure 3.6 Solidify Pattern and Temperature DIstribution 37
Figure 3.7 Second Dendrite Arm Spacing vs Growth Rate 38
Figure 3.8 Thermo Scientific Lindberg/Blue M Moldatherm Box Furace 39
Figure 3.9 LECO Diamond Saw 40
Figure 3.10 Buehler Electro-Polish Machines 41
Figure 3.11 Lecia Optical Microscope 41
Figure 3.12 SEM system 42
Figure 4.1 Sample Positions 44
Figure 4.2 Second Dendrite Arm Spacing 45
Figure 4.3 Statistical Diagram of Second Dendrite Arm Space vs Radial Distance of Selected Area towards the Core Pin 48
Figure 4.4 Silicon Particles 50
Figure 4.5 Diamond-Shaped Particles 51
Figure 4.6 SEM Photographs of Diamond-Shaped Particles 53
Figure 4.7 Line Scanning of Al_2Si_2Sr Particles and Eutectic 55
Figure 4.8 Cross Section of Soldering Areas 56
Figure 4.9 Compositions of Selected Particles 56

Figure Page

Figure 4.10 Backscattered Electron Photographs on Soldering Areas in Group#2 58
Figure 4.11 Spectrums of Selected Spots in Group#2 59
Figure 4.12 Backscattered Electron Photographs on Soldering Areas in Group#3 60
Figure 4.13 Spectrums of Selected Spots in Group#3 61
Figure 5.1 Strontium Particles and Iron particles 63
Figure 5.2 Al-Sr Oxide 64

Appendix Figure

Figure A.1 Energy Table for EDS analysis 72

LIST OF ABBREVIATIONS

BSE	Backscattered Electron
EDS	Energy Dispersive Spectrometer
FDA	Finite Difference Analysis
HPDC	High Pressure Die Casting
SEM	Scanning Electron Microscope

GLOSSARY

Core Pin: A die pin that is used for forming a core in high pressure die casting.

Die Soldering: A metallurgic or chemical reaction between aluminum alloy and steel above eutectic temperature and form intermetallics that joint the casting and the die.

Eutectic: A solid mixture that is formed by two or more metal components at certain proportion and certain temperature.

Segregation: The excessive component is pushed into the grain boundary due to low solubility in matrix alloy. The component aggregates at center area according to the solidification pattern and temperature gradient. The aggregation is defined as segregation.

Undercooling: The temperature of melting alloy is lower than its solidus line and still remains liquid.

ABSTRACT

Pengyu Zhu. M.S., Purdue University, December 2015. Effect of Strontium in Soldering Resistance. Major Professor: Qingyou Han.

Extrusive effect has been taken in the area of die soldering study because such phenomenon is responsible to die failures. Die failure causes huge amount of maintenance cost and machines shutting down. Knowing the mechanism of die soldering and soldering resistance saves not only money but also reduces machine downtime. Industry has found that strontium, instead of iron conventionally, has significant effect in enhancing soldering resistance of H13 steel. Previous studies on strontium effect proposed the ideas that strontium changed the surface tension and wet angle of melting aluminum and also formed a layer on the melting surface. Thus, the diffusion between aluminum and iron was restricted. In this study, the author aimed to discover the oxide layer of strontium and verify the proposals. Approximately 0.03%wt to 0.05%wt of strontium in aluminum alloy can effectively reduce die soldering. In this thesis, the chemical and metallurgical effects of strontium were analyzed. Mold filling experiments and solidification simulation were conducted. Temperature gradient during solidification was studied. Microstructure including distribution of strontium and strontium oxide layer were studied by SEM and BSE. It has been found that strontium is segregated in the eutectic region, forming intermetallic phase and oxide.

CHAPTER 1. INTRODUCTION

Die soldering is a severe die failure mode and a major cause in shortening die life. Die soldering is also responsible for lowering products quality during high pressure die casting (HPDC). Plenty of studies have been done for soldering mechanism (Nabawy, 2001). During HPDC process, the lock force ranges from 200 to 5000 tons and fluid velocity of molten alloy reaches up to 100m/s. Metal die, made of H13 steel, generally suffers from extreme service conditions and die failure occurs after normally 10,000 cycles.

In high pressure die casting, core pins are utilized for forming functional holes in castings. Soldering occurs on gating side due to direct impact of molten metal as well as back side due to flow pattern and flow parameters such as high velocity and pressure. Soldering also results from ineffective water cooling line, because the materials near the core surface is still molten while the pin is ejected. Figure 1.1 demonstrates the soldering area on a core pin: (a) and (b) are soldering areas on a round and a square pin on gating side; (c) and (d) are soldering areas on the back side.

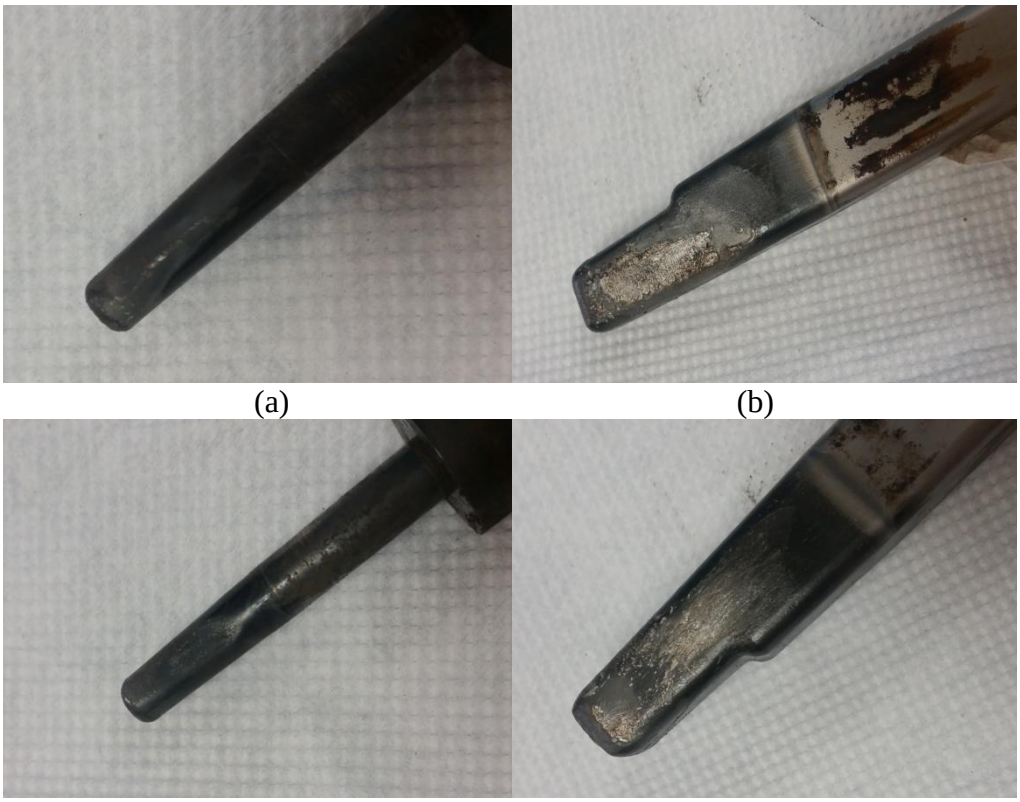

(a) (b)

(c) (d)

Figure 1.1 Die Soldering on Core Pin

Conventionally, iron is used as soldering resistance agent by increasing the iron content in molten aluminum alloys to lower the diffusion of iron into aluminum and reduce the tendency of the reaction between iron and aluminum. On the other hand, however, the mechanical properties, especially ductility, are significantly degraded by a needle-like ternary eutectic phase if Fe-Al-Si.

1.1 Scope

Observations from industry indicated that strontium played an important role in die soldering resistance. Compared with iron, strontium also modified the eutectic silicon phase structure from a plate-like morphology to rosette-like one. Thus, the mechanical properties are improved by the additive of strontium. However, the mechanism for improving soldering resistance by strontium still remains unknown. The object of this

research is to understanding the mechanisms by which strontium works in improving the soldering resistance of H13 steel in molten aluminum alloys.

1.2 Significance of This Research

Die casting aluminum alloys have replaced conventional casting irons for engine blocks to fulfill the requirements for vehicle weight reduction as well as energy economy. Replacement of such critical structure steel parts with aluminum can be achieved with heavier tonnage die casting machines in 5 years. Newly proposed aluminum alloy is required to achieve high mechanical properties such as yield strength, elongation and impact strength. Iron, a critically detrimental component in casting aluminum, forms a needle-like phase and lowers the ductility. However, a concentration of 1.3% max iron is added in aluminum to prevent die soldering, which results in high cost for die maintenance or replacement. The newly proposed low iron and high strontium alloy, a concentration of 0.05%-0.07% strontium replaces iron as soldering resistance additives, achieves high tensile and impact strength. New alloys are labeled as “Mercalloys”.

Mercalloys are claimed to be able to replace existing Al-Si hypoeutectic die casting alloys such as A380 and A360. There newly derived alloys include all current versions of die casting alloys. The proportion of iron is less and the level of strontium is as high as 0.05%-0.07%. Table 1.1 illustrates the component of current Aluminum Association version and new proposed alloys.

Table 1.1 New Proposed alloys

Alloy	Si	Fe Max	Cu	Mn	Mg	Ni	Zn
360	9.0-10.0	2.0	0.60	0.35	0.40-0.60	0.50	0.50
A360	9.0-10.0	1.3	0.60	0.35	0.40-0.60	0.50	0.50
B360	9.0-10.0	0.40	0.25	0.25-0.35	0.40-0.60	0.10	0.10
380	7.5-9.5	2.0	3.0-4.0	0.50	0.10	0.50	3.0
A380	7.5-9.5	1.3	3.0-4.0	0.50	0.10	0.50	3.0
B380	7.5-9.5	1.3	3.0-4.0	0.50	0.10	0.50	1.0
C380	7.5-9.5	1.3	3.0-4.0	0.50	0.10-0.30	0.50	3.0
D380	7.5-9.5	1.3	3.0-4.0	0.50	0.10-0.30	0.50	1.0
E380	7.5-9.5	1.3	3.0-4.0	0.50	0.30	0.50	3.0
F380	8.5-9.5	0.40	3.0-4.0	0.25-0.35	0.10-0.30	0.10	3.0

The new proposed low iron and high strontium version, B360 and F380, achieves high elongation, however cannot be applied for high cost.

The basic Al-Si alloy with a proportion of 0.5-0.8% manganese for soldering resistance is labeled as 365 by Aluminum Association. The newest developed alloy with 11% silicon is labeled as 362, in which the proportion of manganese is 0.25-0.35% and the level of strontium is 0.05-0.07%. The alloys Mercalloy 367 and 368 have the same concentration of manganese and strontium for die soldering resistance with different level of Si, which is 9%, from 365 to achieve different fluidity. The similar fluidity data is also collected in Flow-3D simulation software.

Several newly proposed alloys replace iron with strontium for soldering is labeled below. The components are also illustrated.

- 367.0: 8.5-9.5% Si, 0.25% max Fe, 0.05-0.07% Sr, 0.25% max Cu, 0.25-0.35% Mn, 0.30-0.50% Mg, 0.10% max Zn, 0.20% max Ti, other-each 0.05%, and other-total 0.15%
- 368.0: 8.5-9.5% Si, 0.25% max Fe, 0.05-0.07% Sr, 0.25% max Cu, 0.25-0.35% Mn, 0.10-0.30% Mg, 0.10% max Zn, 0.20% max Ti, other-each 0.05%, and other-total 0.15%
- 362.0: 10.5-11.5% Si, 0.40% max Fe, 0.05-0.07% Sr, 0.20% max Cu, 0.25-0.35% Mn, 0.50-0.7% Mg, 0.10% max Ni, 0.1 0% max Zn, 0.20% max Ti, 0.10% max Sn, other-each 0.05%, and other-total 0.15%

Conventional alloy using iron or manganese for soldering resistance are based on the theory of super-saturation. High level of iron or manganese lowers the diffusion between molten alloy to die and thus decrease the formation of soldering. The newly proposed alloys, however, is claimed to rely on surface modification of strontium. The additional strontium is supposed to create a surface film between alloys and dies with only 1/10 the concentration of iron. The film functions as a barrier and prevents the reaction. However, a paper by NADCA, named Avoiding Washout in Shot Sleeves When Used with Low Iron, Structural Aluminum Die Casting Alloys, illustrated that the oxide film formed by strontium is under static condition. In shot sleeve, however, where dramatic change in pressure and turbulence occur frequently. The thin oxide film can be easily broken and the diffusion between iron and aluminum occurs. The erosion of shot sleeve can be severe with low iron high strontium alloys.

1.3 Research Question

The basic idea of the research is to figure out the answers to the following questions:

- What's the segregation behavior of Sr and its compound during solidification?
- Will the dissolution of Sr decrease the solubility of Fe in A380 melt?
- What's the morphology of Sr containing phases?

1.4 Assumption

The following assumption were inherent to the pursuit of this study:

It was wildly accepted that die-soldering can be significantly reduced by additive strontium into the A380 alloys. However, little work has been performed on the mechanisms of soldering reduction with strontium. Therefore, it is necessary to explore the mechanisms of soldering resistance by studying the structure and morphology of the phases near the alloy-steel interface using optical microscope and Scanning Electron Microscope (SEM) and chemically by studying the components of the soldering area using Energy Dispersive Spectrometer (EDS).

1.5 Limitations

Due to the conditions and the equipment of the research, there are several limitations:

- The study was limited to one type of alloys-A380 alloys.
- The accuracy of the proportion of components relies on the accuracy of the instrument such as EDS.

1.6 Delimitations

Due to the research questions, there are several delimitations:

- The research focused on the proportion and the distribution of strontium to indicate the segregation of the strontium, besides, the morphology of the Al-Sr compound was studied.
- The quality and quantity of the data were accurate to distinguish the component and morphology difference of different areas of soldering layer.
- The instruments for experiments work correctly and control the variable such as temperature, testing time, proportion of strontium.

1.7 Summary

This chapter has described the main motivation of the study as well as the scope, significance and research question. Also, lists of assumption, limitations and delimitations have been provided. The next chapter presents a brief summary of relevant literature related to A380 eutectic structure as well as soldering mechanism.

CHAPTER 2. LITERATURE REVIEW

2.1 Outline

Aluminum is utilized for substituting conventional heavier materials such as steel and cast iron in vehicle manufacture to satisfy the requirements for fuel economy and emissions reduction. Al-Si-Cu casting alloys, labeled A380, are significantly light metals that are widely utilized as automotive components due to their proper mechanical properties as well as castability. Usually and conventionally, the mechanical properties, such as strength and ductility, of the product can be improved by carefully control the solidification microstructure, including second dendrite arm spacing, grain size and eutectic silicon morphology. Commonly, component products, such as transmission case and oil pan are processed by high pressure die cast. In HPDC, velocity is about 50–100 m/s during the mold filling process and the pressure is about 70MPa which impose a severe condition for dies during and after the mold filling. Die soldering is a major die failure mode and is a major cause for reduced die life and production downtime.

2.2 Die Soldering

During HPDC process, soldering occurs when molten aluminum sticks with die steel. Such phenomenon results in washing out surface material of the die and detrimental surface quality of the casting, as well as shut-down time for product quality control and die maintenance. Soldering occurs through chemical/metallurgical reaction and mechanical impacts. Intermetallic layers are formed in soldering reaction. However, such

intermetallic layers can be degrade and causes soldering to cast aluminum and shortens die life.

2.2.1 Die Soldering: Introduction and Back Ground

Currently, die soldering has caused lots of research interest in the die casting industry. According to the research of Nazari. K. A (2009), soldering reaction is related to diffusion between aluminum and iron as well as kinetics reaction potential between Al and Fe.

Conventionally, iron is intentionally added into molten aluminum alloys for soldering resistance agent by raising the bulk concentration of iron in the alloy that not only retards diffusion between die and alloys, but also significantly decreases the solubility of iron in aluminum that can diffuse from the die to molten. Another research by Domkin. K (2009) related the addition of Fe to diffusion control in aluminum high pressure die casting. The higher iron content reduces the rate of the interfacial reaction, which is consistent with a thinner intermetallic soldering layer. This can be explained by super saturation theory that the iron in the melt becomes saturated, which reduced the reaction potential between Al and Fe. A lower driving force to such a reaction results in the formation of a thinner intermetallic layer. On the other hand, however, increasing the iron level in liquid causes the formation of iron-bearing intermetallic compounds in the cast structure. Fe is the most detrimental impurity element in casting aluminum because of its role in the formation of a brittle intermetallic compound, Al_5FeSi, labeled as β-phase. The mechanical properties, especially ductility, are significantly reduced by a needle-like ternary eutectic composition of Fe-Al-Si. Thus, iron is not recommended in high pressure die casting in terms of mechanical protection of the aluminum casing.

2.2.2 Die Soldering Reaction

The typical composition of die soldering layers was given by Joshi in 2002, and is demonstrated in Figure 2.1. The alloy matrix A390 is located at the top of the image and H13 steel die is located at the bottom of the image. The intermetallic layers, consisting of aluminum iron and silicon with different proportions, are proceeding towards the H13 die. The concentration of iron increases in the layers from A390 alloy to H13 substrate.

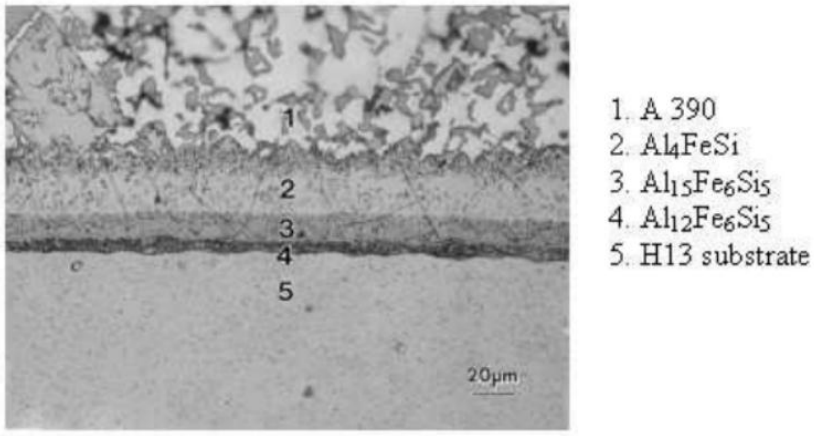

Figure 2.1 Intermetallic Layers of Soldering on H13 Steel Die

The component and proportion of die soldering layers vary depending on the composition of the aluminum alloys and the steel die.

Two types of soldering mechanism were characterized by previous studies (Y. L. Chu & P. S. Cheng, 1993). One occurs at high temperatures due to the chemical or metallurgical reaction between the molten alloys and the steel die and the other occurs at low temperature when molten aluminum impacts on the die surface at high velocities. The first type of die soldering is related to the washout of the surface protective materials of steel die. During high pressure die casting process, rapid contacts between molten alloys and steel die occurs and surface protective materials, coating or die lube for

example, have been washed out. Directly contact with molten aluminum alloy on die surface results in severe diffusion and reaction between steel and aluminum at high temperature. Thus, intermetallic layers are formed on die surface and solid joints are formed on cooling. During the ejection of casting from the die, surface materials of steel die will be tore out and repetition of the process eventually results in die failure.

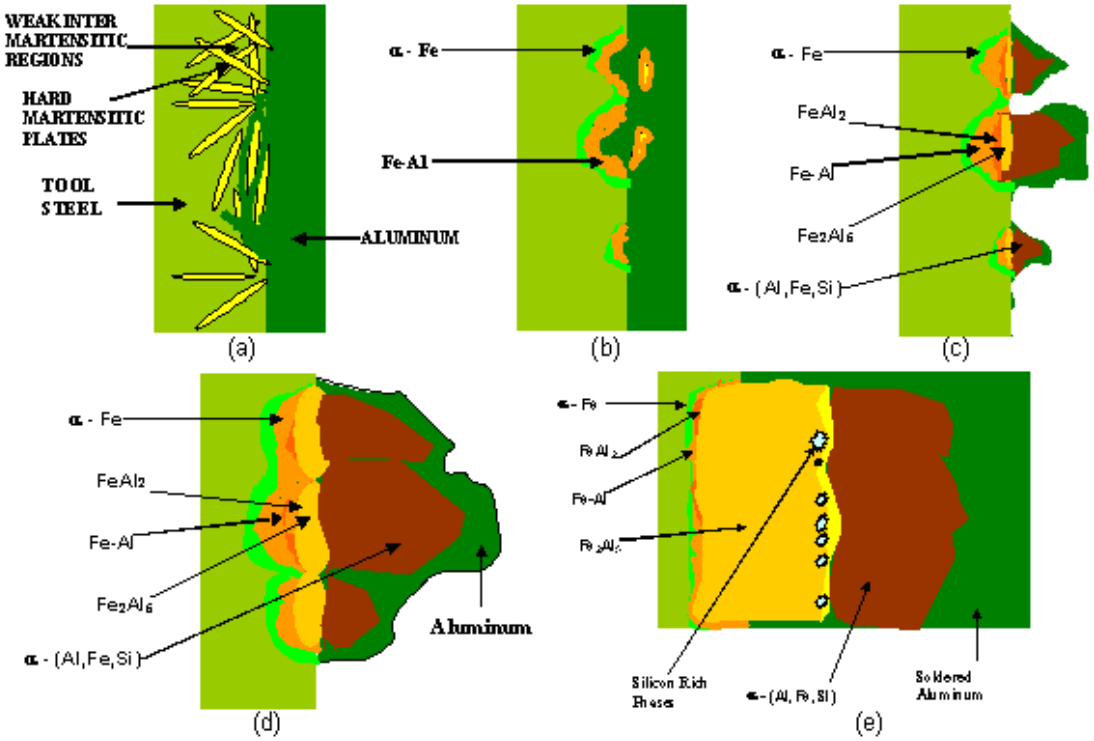

Figure 2.2 Schematic Illustration of the Formation of Intermetallic Layers at the steel/Al interface

Figure 2.2 schematically demonstrates the process of forming intermetallic layers at the steel/aluminum interface. A six-stage process was proposed by Shankar in 2002.

- Erosion of grain boundary on the die surface. Erosion begins at the weak inter-granular martensitic regions between hard martensitic plates. Solid solutions of iron and aluminum are formed in these areas.

- Pitting on the die surface. Semi-spherical pits are formed on the surface of the die due to multiple impacts and erosion of a molten alloy at high pressure and high velocity in gating areas as well as core pin areas.
- Formation of Al-Fe compounds. Compounds with the chemical proportion: FeAl, $FeAl_3$ and Fe_2Al_5 start to form at the surface of the pits. During high pressure die casting process, each shot accumulates the growth of these compounds.
- Formation of α-(Al, Fe, Si) phase. The participation of silicon in the reaction between iron and aluminum results in a pyramid-shaped α-(Al, Fe, Si) phase. Growth of the pyramid-shaped phase is preferential and dominated by the diffusion of iron.
- Aluminum sticking onto α-(Al, Fe, Si) phase. The reaction between aluminum, silicon and iron entraps aluminum atoms to the intermetallic layers.
- Growth of intermetallic layers and merging of neighboring pits. Intermetallic layers begin to expand and merge neighboring pits. Molten alloy encounters the die surface.

2.2.3 Critical Temperature for Soldering Reaction

Dipping experiments were conducted by Q. Han and S. Viswanathan (2003), in which a mild steel cylinder was dipped into pure aluminum melting at different temperatures for different time. Results from BSE (backscatter electron) images indicated that eutectic and $FeAl_3$ compound were found at intermetallic layers. The phase diagram of aluminum and iron, shown in Figure 2.3, indicates that the eutectic reaction:

$$L = Al + FeAl_3$$

occurs above 655℃. One eutectic phase is an aluminum-rich liquid when the content of aluminum is greater than 61.3%wt. On cooling, this liquid phase freezes into solid phase and is responsible for the formation of Al-Fe bonds that joints the aluminum casting and the die.

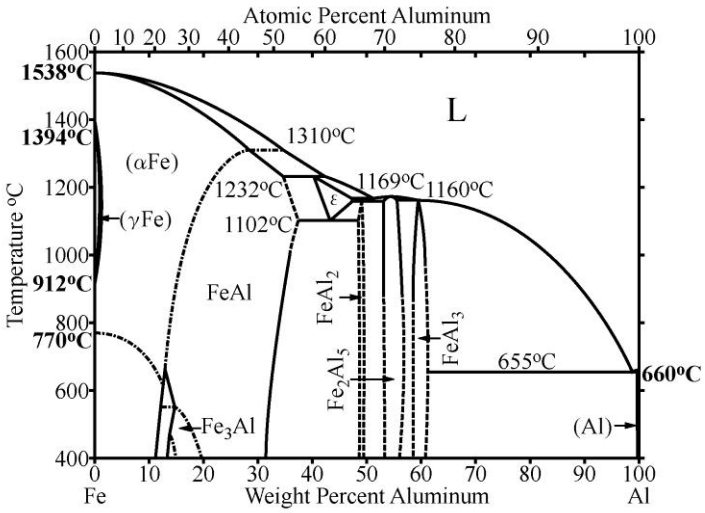

Figure 2.3 Al-Fe Phase Diagram

During high pressure die casting process, iron diffuses into the molten alloy liquid and the concentration of the iron is initially low. The diffusion rate of iron will be restricted as iron becomes saturated in alloy and intermetallics begin to form on the surface of the die. On the other hand, the diffusion of aluminum into the die enriches aluminum at the die surface and, thus, expands the thickness of the intermetallic layers.

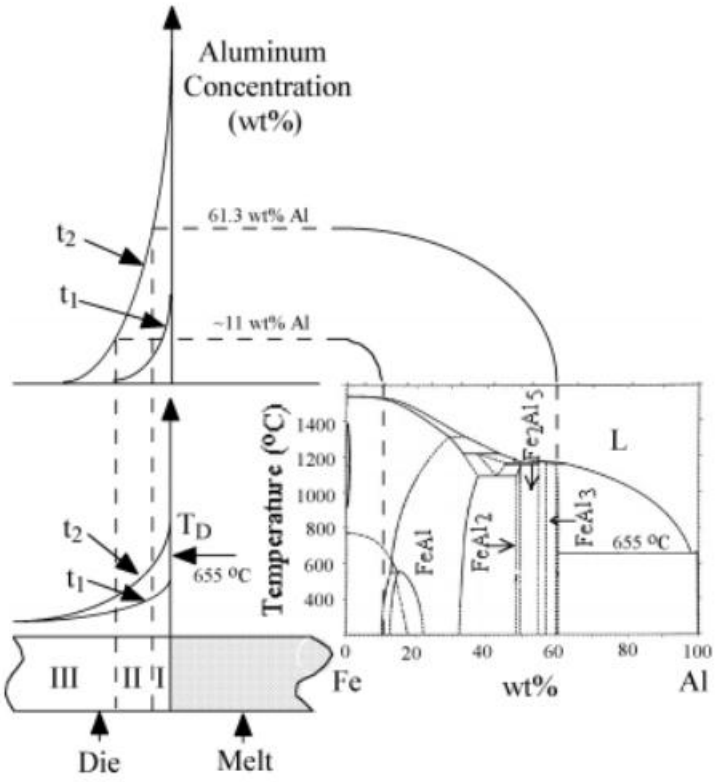

Figure 2.4 Schematic illustration showing possible aluminum composition and temperature profiles at the die surface.

The formation and expansion of intermetallic layers is schematically demonstrated in Figure 2.4. Time points of diffusion are denoted by t_1 and t_2. As time increases from t_1 to t_2, the proportion of aluminum that is diffused into the die increases. The composition at t_2 in region Ⅰ is illustrated in the phase diagram. The concentration of aluminum in region Ⅰ is greater than 61.3%wt because this region contact directly with aluminum. The solidus temperature of aluminum is higher than eutectic temperature, 655℃ according to the phase diagram. Thus, $FeAl_3$ and aluminum-rich phase are formed. Such phases play an important role in die soldering because the aluminum-rich phase can be a liquid phase at die casting temperatures. During cooling process, the liquid

aluminum-rich phase solidifies first and joint casting and steel die. According to the phase diagram, when the proportion of the liquid phase is large enough, the joint will be strong enough and severe soldering will be formed. As a result, surface materials on the die will be tore off during the ejection. In one word, the critical temperature for die soldering formation between pure aluminum and steel die is 655℃. The value varies depending on the alloys and the composition of the die steel.

2.3 Properties of A380 Aluminum Alloy

The eutectic systems, combined by two or more pure metals, have been used for several centuries for casting engineering components and structural components. The research of Makhlouf. M. M (2001) suggested that, such eutectic mixtures result in lower melting temperature as well as higher mechanic properties. Aluminum-silicon, iron-carbon systems are frequently used systems.

2.3.1 Al-Si system

The aluminum-silicon eutectic system has been studied for decades since 1921 and some of current understanding towards the reaction has been developing into many new types of aluminum alloys with different properties and applications.

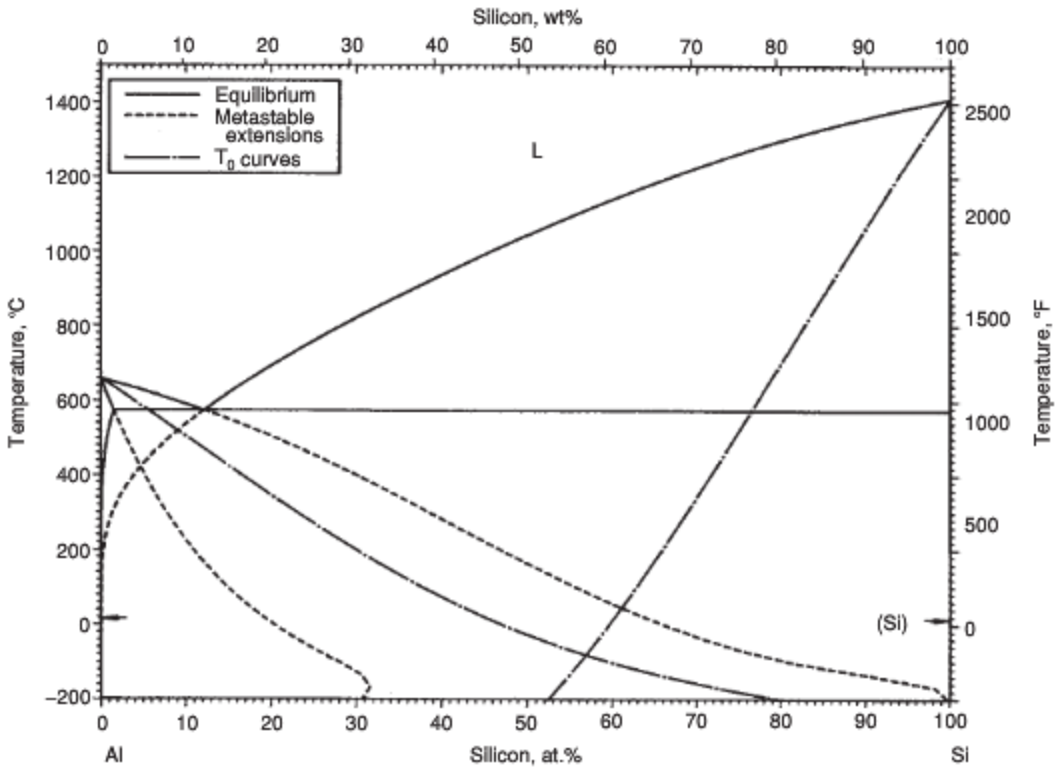

Figure 2.5 Al-Si Equilibrium phase diagram

Liu (2001) studied the influence of alloy elements on the mechanical properties of Al-Si alloys. Some of his research result is illustrated in Figure 2.5 that the maximum solubility of silicon in aluminum is about 1.5 at. % at eutectic temperature; and the solubility of aluminum in silicon is nearly zero. It is generally accepted that the eutectic reaction occurs at 577℃ with the concentration of silicon at about 12.6 % wt. In practice, however, the eutectic structure forms at 10 to 12℃ below the eutectic temperature due to the fact that primary silicon undercools more than primary aluminum.

Different cooling rates also result in different morphologies of the eutectic structure. The microstructure of a eutectic aluminum-silicon alloy that is slowly cooled and shows no primary aluminum; on the other hand, the micro-structure of the same alloy

cooled at a significantly faster rate and shows primary aluminum dendrites and finer silicon particles.

2.3.2 Morphology and Properties of α-phase and β-phase

The unmodified eutectic microstructure is characterized by coarse and needle-like silicon particles. Such morphology is achieved by lower cooling rates and no chemical additives treatments such as strontium and manganese.

Contemporary understanding of eutectic formation is based on the fact that invariable containing of iron is inevitable in aluminum-silicon alloys (Patakham, Ussadawut, Julathep Kajornchaiyaku and Chaowalit, 2013). Therefore, the eutectic structure is a combination of Al_{eut} + Si_{eut} + β. The β-phase significantly contributes in the nucleation of aluminum and silicon eutectic structure. The structure is demonstrated in Figure 2.6.

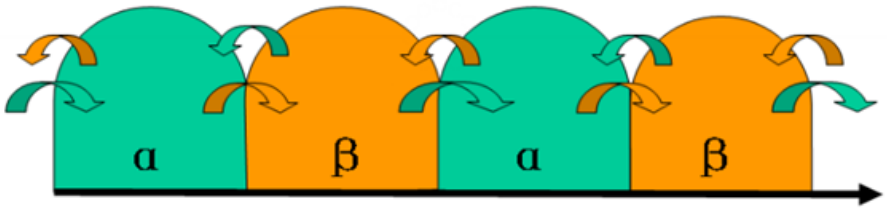

Figure 2.6 Interleaved Structures

During the solidification, the primary aluminum phase, denoted as α-phase, are separated from the liquid as dendrites. The new formed β-phase acts as nucleating agent for silicon eutectic at an undercooling of 0.4 to 0.8℃ at eutectic temperature. Once nucleated, the affiliation is enriched with aluminum; consequently the aluminum nucleates and grows on the edge of silicon eutectic. A final interleaved structure

consisting of α-phase and β-phase will be formed. The present of β-phase results in lower mechanic properties such as lower ductility due to its needle-like morphology. Thus, chemical treatments are always applied to modify the morphology of the microstructure.

2.3.3 Si-Sr Diagram

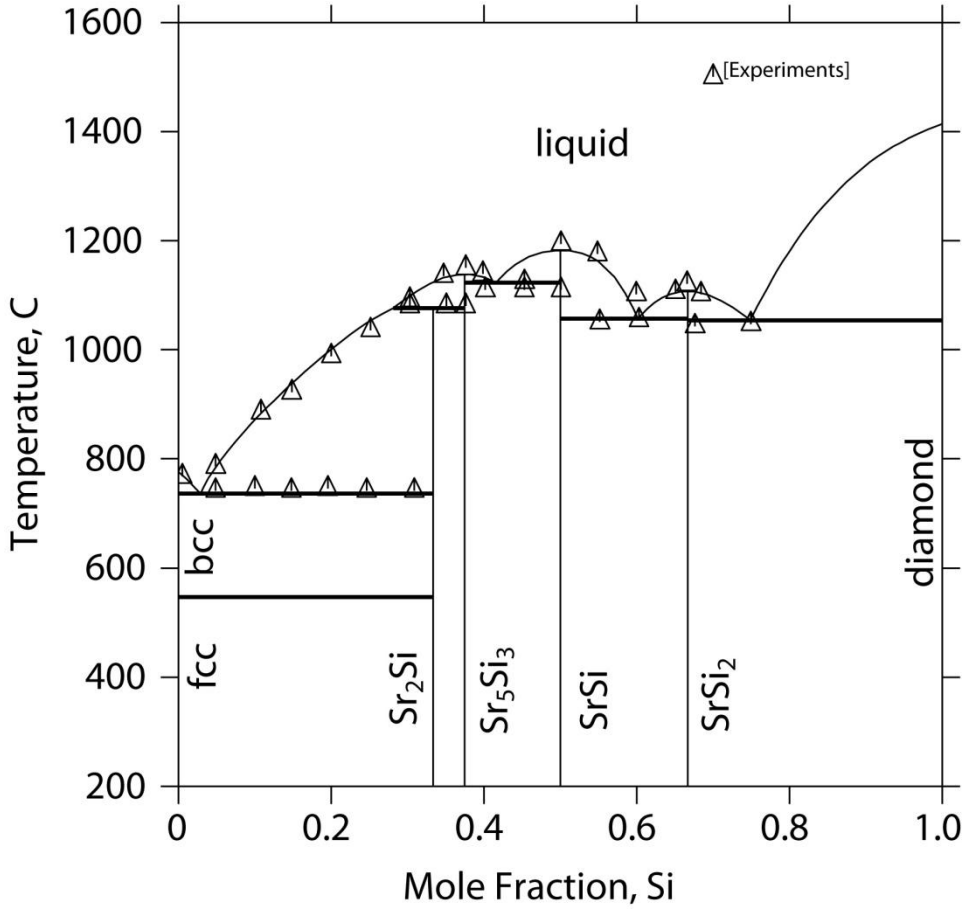

Figure 2.7 Si-Sr Phase Diagram

Silicon-Strontium phase diagram was predicted by Computational Material Science Lab using CALPHAD approach. Figure 2.7 demonstrates the predicted phase diagram of silicon-strontium system. Mole fraction was used as X-axis to indicate the molecular formula of the phase. According to the diagram, the solubility of silicon in strontium is nearly zero. Also, strontium and silicon are unable to form a solid solution

during a high pressure die casting process which occurs at high temperature between 630℃ and 650℃.

2.3.4 Al-Si-Sr Intermetallics

First-Principles calculation, derived by the Density Functional Theory, was used for categorizing Al-Si-Sr intermetallic theoretically (A. M. Garay-Tapia, 2013). Totally twelve ternary intermetallics were explored and the stability of the intermetallics were determined mechanically and energetically. The elastic constants as well as the calculated enthalpy were utilized for the determination. Two approximations for the cell parameter calculation were applied. These are Local Density Approximation (LDA) and Generalized Gradient Approximation (GGA). The chemical formulas of the ternary intermetallic are given in Table 2.1.

Table 2.1 Al-Si-Sr Ternary Intermetallics

Phase	ΔH_f^{LDA}	ΔH_f^{GGA}	Cell Parameters		
			Expected Value		
			a	b	c
AlSiSr	-40.85	-43.43	4.23	4.23	4.74
Al_2Si_2Sr	-31.00	-31.38	4.18	4.18	7.41
$Al_2Si_2Sr_3$	-42.05	-43.34	4.07	4.82	19.00
$Al_{16}Si_{30}Sr_8$	-16.00	-16.20	10.47	10.47	10.47
$Al_2Si_3Sr_3$	-40.29	-36.56	11.85	4.45	15.36
$Al_2Si_4Sr_3$	-43.18	-38.41	12.48	4.15	8.75
$Al_2Si_7Sr_5$	-42.87	-38.02	8.23	9.83	17.80
$Al_3Si_7Sr_{10}$	-42.48	-40.41	9.34	9.34	15.74
$Al_6Si_{13}Sr_{20}$	-39.91	-37.35	16.77	4.76	16.70
$Al_6Si_9Sr_{10}$	1.90	2.10	14.39	14.39	22.00
$Al_8Si_3Sr_{14}$	-29.01	-29.13	11.96	11.96	39.92
$AlSi_6Sr_4$	5.55	7.17	19.98	4.00	7.02

The calculation of formation enthalpy was given in the following formula: $\Delta H_f^{AlxSiySr1-x-y} = E^{AlxSiySr1-x-y} - X \cdot E_{Al}^{Fcc} - Y \cdot E_{Si}^{Dia-A4} - (1 - X - Y) \cdot E_{Sr}^{Fcc}$ in which E_{Al}^{Fcc}, E_{Si}^{Dia-A4} and E_{Sr}^{Fcc} are energies of aluminum, silicon, and strontium in intermetallics with higher stability at 0K. Besides, $E^{AlxSiySr1-x-y}$ denotes total energy of the compound at 0K. The negative formation enthalpies indicate that the phases achieve

energetic stabilities. The ground state of the Al-Si-Sr intermetallic would be the phases with the lowest enthalpy. Thus, AlSiSr and $Al_2Si_2Sr_3$ phases, according to Table 2.1, are most likely the ground state of the system.

The structural feature of the Al-Si-Sr ternary system was proposed according to the known analogous Al-based prototype ternary system such as Al-Ge-Ba, Al-Ge-Sr and Al-Si-Mg. The Al-Si-Sr ternary system contains a global skeleton of Al-Si bounds with strontium atoms aggregated in the surroundings. The average length of Al-Si bounds is 2.46 ± 8 Å and the angles of Si-Al-Si have an average of 116.5 ± 10º. The distance between strontium atoms ranges from 3.32 Å to 4.69 Å.

2.4 Segregation behavior of Strontium

Segregation occurs during solidification, describes the non-uniform distribution of additive elements in alloy matrix. The casting solidified in general condition, room temperature and pressure, consists of four zones. Figure 2.8 illustrates four different zones in a solidified casting.

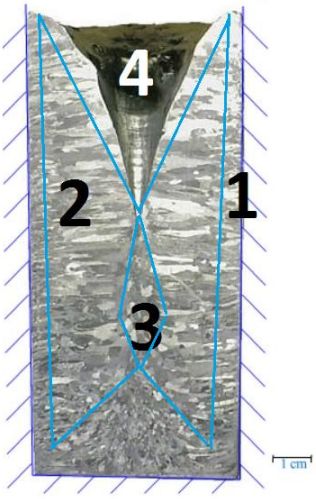

Figure 2.8 Solidification Zones

- Chill zone (1) – Solidification initiates at the chill zone due to the low temperature of the mold wall. High cooling rate results in nucleation in random orientation and prevents grains from growing.
- Columnar zone (2) – The crystallographic axes of grains are parallel in the direction of the temperature gradient. Such grains grow towards the center of the mold at the expense of grains aligned in other directions.
- Equiaxed zone (3) – Equiaxed zone is the last area to solidify in the center of the casting parts. Fine grains nucleate heterogeneously. This is desirable as the small grains reduce micro-segregation.
- Shrinkage (4) – The density of solid is higher than liquid. Liquid compensates volume loss during solidification. Thus, shrinkage occurs at the last solidifying area.

Crystallization occurs with undercooling. Nucleation energy is notated as ΔG^* and is defined by the formula:

$$\Delta G^* = 16\pi\sigma^3 Tm^{2/3}(Lm\Delta T)^2$$

where ΔT denotes the undercooling rate.

Nucleation rate, I, is denoted as I and defined by the formula:

$$I = K \times \exp(-\Delta G^* + \Delta ED)/kT$$

Form the above formulas, it can be seen that nucleation energy decreases with the increase of undercooling rate and increases with the increase of undercooling rate.

Figure 2.9 shows the Phase diagram of Al-Sr. The phase diagram indicates that the solubility of strontium in aluminum is at a very low level. The eutectic structure is

formed at around 937.63K (663.48℃) with the concentration of strontium less than 0.05%.

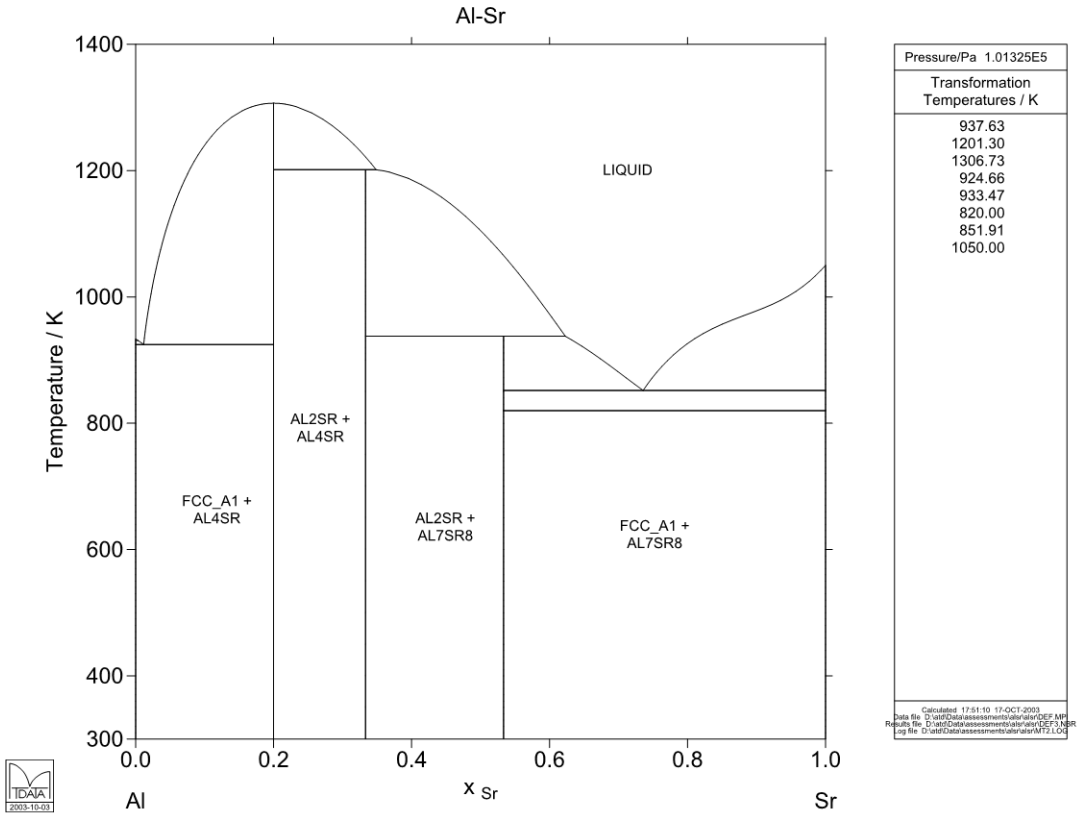

Figure 2.9 Al-Sr equilibrium phase diagram

In the temperature ranging from 803-823K, which is the general filling temperature range in a HPDC process, strontium is segregated as Al_4Sr with a FCC matrix. In manufacturing application, 0.05% of strontium is added to aluminum alloys such as A380 to prevent die soldering. (Adam Kopper and Dr. Raymond, 2006) According to the lever rule, the proportion of strontium in the primary dendrite and second dendrite follows the solidus and additional strontium will be pushed into the liquid. The diffusion process of a binary system follows the formulas:

$$K_e = K_0 / (K_0 + (1-K_0)\, e^{-R\delta/D})$$

$$C_S^* = K_0 C_0 / (1 - f_S)^{(K_0 - 1)}$$

C_S^* is the concentration of solute in a solid phase; f_S is the percentage of solid phase in the system; K_e is the effective distribution coefficient; K_0 is the equilibrium distribution coefficient of equilibrium solidification. The coefficient Rð/D is nearly zero when the solidifying rate is high. Figure 2.10 illustrates a schematic of the equilibrium solidification process. The shaded part of the rectangle indicates the solid component. The concentration of solute, strontium in this case, in solid phase is lower than that in liquid phase, as is indicated in the first diagram. Thus, additional solute is pushed into the liquid phase and aggregated at the liquid/solid front. As solidification proceeds, the concentration of solute in liquid phase increases and results in a higher concentration of solute in the solid phase. The solid phase achieves saturation during the solidification. Additional solute will be finally segregated at the last solidifying area.

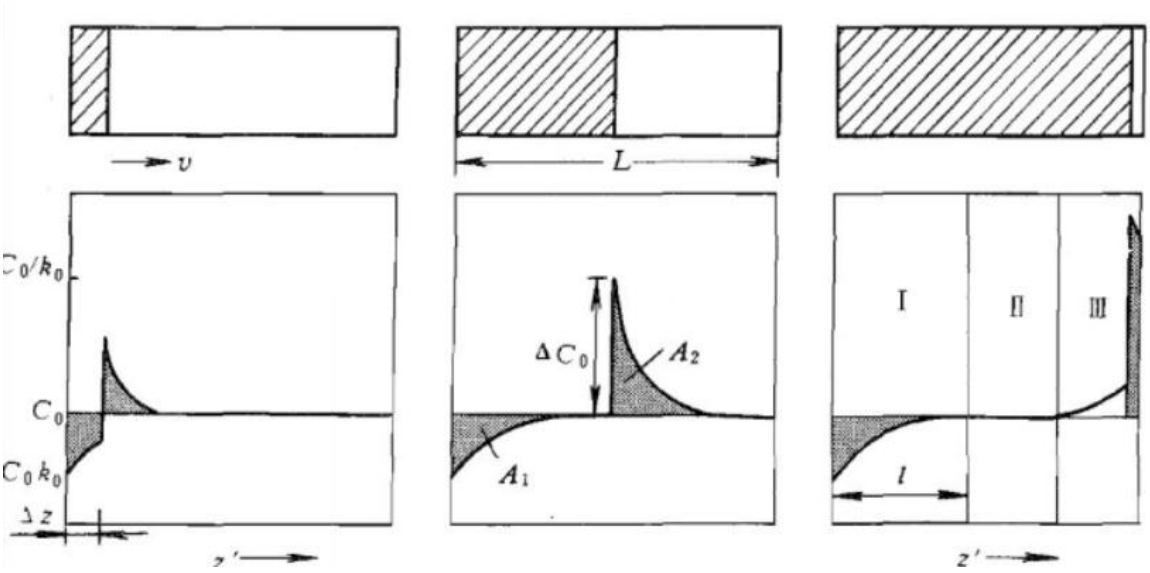

Figure 2.10 Component Diffusion Process

2.5 Strontium Effect

Observations from manufacturing applications indicate that strontium also plays an important role in die soldering resistance (Chen. Z. W, 2005). Compared with iron, the phase structure is also modified by strontium addition from a tough and needle-like morphology to a smooth and round one. Researchers have shown that the Sr-modified alloy results in higher values of elongation and impact toughness compared to the unmodified alloy. Thus, the mechanical properties were improved by the presence of strontium. This is the reason why strontium is preferred as a soldering resistance agent (Tavitas-Medrano. F. J, 2008).

According to the research of Clapham, L (1988), the modified structure of the silicon phase with different concentrations of strontium in A380 alloy is shown in Figure 2.5. The needle-like silicon particles predominantly take up the silicon eutectic structure. By adding an element such as strontium, the modified structure is shown in the subsequent figures, in which the morphology of the silicon particles tends to be less coarse. Thus, higher ductility can be achieved by such treatment. Besides, strontium also acts as a resistance agent for die soldering, an interface reaction between the aluminum alloy and the die, thus resulting in the shortening of die life.

Adam Kopper and Dr. Raymond post an assumption in the paper “Soldering Resistance Mechanisms of Novel Al-Sr-Si Die Casting Alloys” that the strontium additive significantly decreases the contact angle between aluminum and H13 die steel, which, in high concentration, creates a non-wetting condition. Besides, a barrier is formed on the contact surface between the casting alloy and die’s steel, thus decreasing the diffusion and soldering reaction between the aluminum and iron. The alloys used for

research is Mecalloy 366 and 367. The compositions of Mercalloy 366 and 367 are illustrated in Table 2.2.

Table 2.2 Composition of Two Mercalloy alloys

Alloying Element	Mercalloy 366 Composition Weight %	Mercalloy 367 Composition Weight %
Si	9.0 - 9.5	9.0 - 9.5
Sr	0.05 - 0.07	0.05 - 0.07
Mg	0.10 - 0.20	0.35 - 0.45
Fe	0.20 max	0.25 max
Cu	0.15 max	0.15 max
Mn	0.25 – 0.35	0.25 – 0.35
Al	Balance	Balance

From the table data, it can be seen that the proportion of strontium exceeds the typical additions for morphology modification, which range from 0.01 – 0.02%. The excess strontium may result in porosity in sand mold and permanent mold casting because strontium adsorbs hydrogen in the melt and releases it during solidification. Figure 2.11 illustrates the modification of porosity in permanent mold casting due to strontium. The macro-porosity dominated by shrinkage is modified into less harmful micro-porosity. In a HPDC process, however, intensification pressure is enough to minimize the released gas, thus higher level of strontium can be applied for the above postulated purpose.

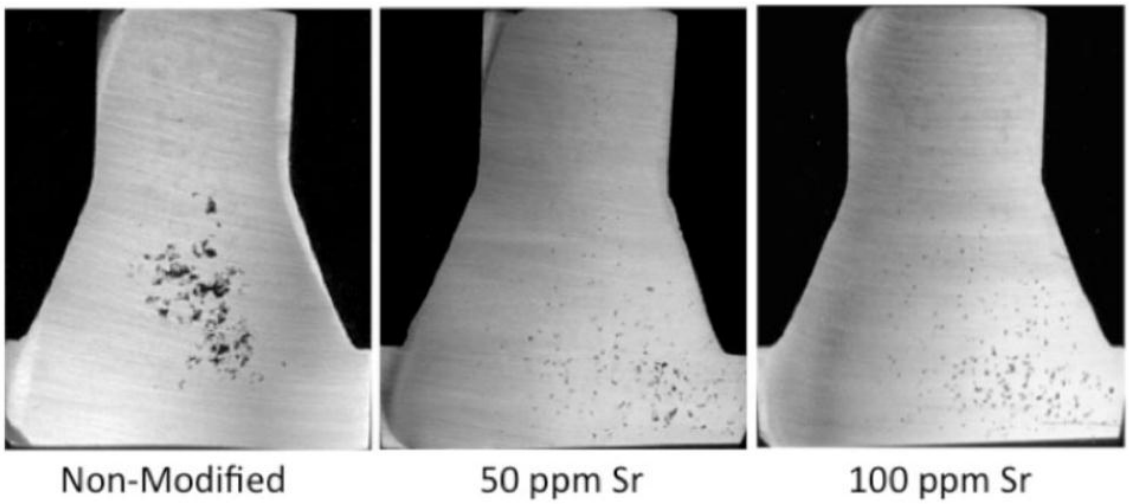

Figure 2.11 Porosities Modified by Strontium

The assumption posted in the paper by Sumanth and Makhlouf based on their research reports about the eutectic microstructure during solidification process of hypoeutectic Al-Si system. The report mentioned that the proportion of strontium was relatively high in inter-dendritic regions and in mushy zone at the end of solidification. The segregation of strontium creates significant undercooling of the melt and results in super-saturation of silicon at the solid front. Primary silicon particles nucleate ahead of the dendrites and create a barrier between the Al dendrites and the liquid. As solidification proceeds, the new-formed barrier may extend to the surface between castings and die steels. The barrier significantly decreases the diffusion or penetration level of aluminum and iron, thus preventing the occurrence of soldering.

Assumptions have been made that the segregation and adsorption of strontium in aluminum contribute to die soldering resistance. First, strontium acted as a surface active element and was absorbed on the surface of the primary phase to provide a barrier for the dissolution of iron. Second, the addition of strontium causes a super-saturation of the

element Fe and Si. Thus, the needle-like ternary eutectic phase precipitated before the primary phase in the liquid. And finally, Fe was rejected into the residual liquid during the solidification and strontium was absorbed on the nucleation sites of the ternary phase, thus, reducing the amount of the phase.

2.6 Summary

This chapter focused on the theoretical concept involving the soldering mechanism of aluminum alloys with steel die. The theories of segregation behavior as well as solidification were discussed both qualitatively and quantitatively. Applications involving industrial products of strontium modified alloys were also discussed in this chapter.

CHAPTER 3. METHODOLOGY

The purpose of the research is to determine the effect of strontium on soldering resistance. Thus, the solidification structure, micro-morphology and chemical components will be studied. A finite difference analysis simulation was conducted using Flow-3D Casting software to obtain the temperature distribution and flow-solidifying pattern of the alloys.

Mold filling tests were conducted in the research. Cylindrical bars made of hot worked tool steel with 0.5 inch diameter were cut into 13 inch lengths. The cylindrical steel bars were used as core pins for a soldering test with melt alloy. During the test, the bar was inserted vertically into a hollow permanent mold. The cylindrical steel bar is shown in Figure 3.1. The bar was preheated to 700℃ in the furnace and inserted in the middle of the mold. However, considering heat transfer between surroundings and the test bar, the temperature of the test bar is expected to drop to 450 to 500℃ before the mold is filled.

Figure 3.1 Testing Cylindrical Steel Bar

In the experiment, an A380 alloy with different concentrations of strontium was molten and mixed in a graphite crucible. After stirring and holding at a constant temperature for 15 minutes, the melt was poured into a permanent mold at approximately 650℃. The chemical composition of the A380 aluminum alloy used in the tests is given in Table 3.1.

Table 3.1 A380 Components

Cu	Si	Fe	Mn	Zn	Ni	Sn	Other	Al
3.0-4.0	7.5-9.5	1.3max	0.1max	1.0max	0.5max	0.35max	0.5max	Remind

In addition, finite difference analysis simulation was conducted using a Flow-3D Casting software to predict flow patterns and solidification patterns of the molten aluminum. Pouring temperature was set at 650℃ and the temperature of the test bar was set at 450℃. Test results shall include the distribution of temperature gradient during filling and solidification. The predicted results from the software will serve as indicators for sample selection on physical experiments.

3.1 Sample Approach

This section discusses the sample approach used in the physical experiment. The purpose of the physical experiment was to simulate the extreme condition for strontium to segregate. Although high pressure compared to HPDC process could not be achieved, solidifying patterns could be manually controlled by carefully setting boundary conditions such as initial temperature and holding temperature. The materials and procedures of the physical experiments will more be discussed.

Approximately three hundred and fifty grams of A380 aluminum alloy was melted in a graphite crucible in each experiment. Strontium was added to the melt at 700℃ and stirred with a graphite bar for 5 minutes to achieve component equilibrium. The mixture was held at 650℃ for 15 minutes to achieve thermal equilibrium. The melt was poured into a permanent mold at room temperature. A steel bar, preheated to 700℃, was inserted at the center of the mold. Figure 3.2 shows the permanent mold used for the experiments. The permanent mold consists of two semi-cylindrical molds that allows casting to be easily ejected by opening the mold.

Figure 3.2 Permanent Mold

The experiment set is shown in Figure 3.3. Mold filling experiments were conducted under the same condition. Pouring temperatures were controlled around 650 to 665℃. Pouring was carried out by the same person. Casting was ejected from the mold after solidifying for 24 hours and cut perpendicularly to observe microstructure along the transversal radius.

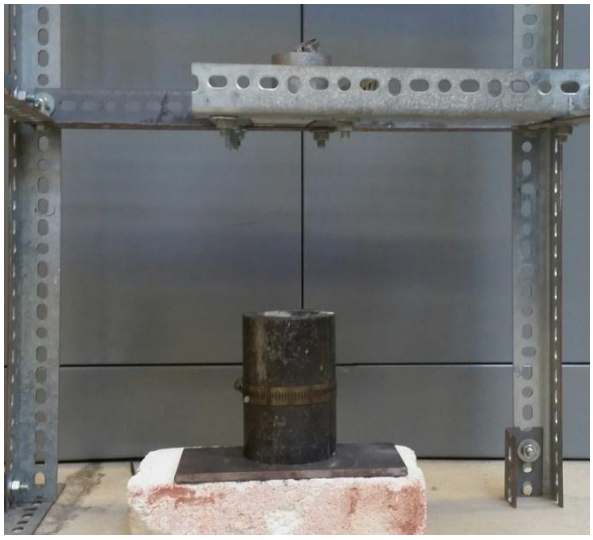

Figure 3.3 Experiment Set

Figure 3.4 shows the ejected sample from the permanent die. White lines indicate the cutting lines. In order to observe the transversal microstructure, specimens needed to be mounted, ground, polished, and prepared for microstructural study. The mounted specimens are shown in Figure 3.4.

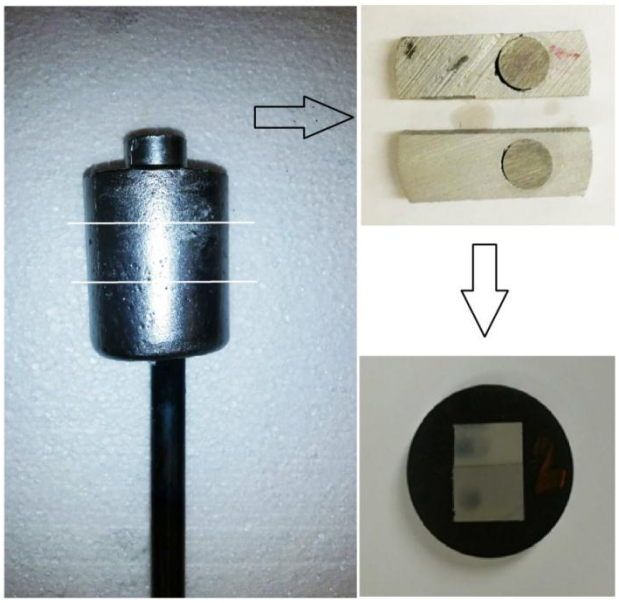

Figure 3.4 Sample Approach

Three groups of samples were made with different concentration of strontium. The compositions of each group as well as the pouring temperatures are illustrated in Table 3.2. Strontium was added through an $Al_{10}Sr$ alloy in which the concentration of strontium is 10%wt.

Table 3.2 Compositions and Pouring Temperature

	A380 (g)	Strontium (g)	Temperature (℃)	Percentage of Sr (wt%)
Group #1	356	1.087	662	0.03
Group #2	359	1.806	655	0.05
Group #3	351	2.490	660	0.07

3.2 Research Hypothesis

The difference in concentration and distribution of strontium on a soldering layer indicates the segregation behavior of strontium and it may also partly explain the effect of the presence of strontium on soldering resistance. The solidifying rate and direction are indicated by second dendrite arm spacing. Three groups of samples were made using concentrations of 0.03%, 0.05%, and 0.07% of strontium. Hypotheses are made as follows:

- Solidification occurs from the permanent mold boundary to the center. Areas around the test bar are location of the last solidification.
- Strontium is segregated at the grain boundary and Sr-rich particles can be found in the eutectic structure.
- The concentration of strontium increases from the mold boundary to center.

3.3 Data Collection

Two sets of quantitative data were collected during the testing. These include concentration of strontium on selected areas and second dendrite arm spacing. Multiple areas locations were selected along the transversal radius and the concentration of strontium and second dendrite arm space were measured at the locations. Diagrams and tables of data distribution are presented and discussed. Two variables, which were served as initial conditions, are shown to have dramatic influence on the testing result. These include the initial proportion of strontium added to the melt and the initial temperature of the test steel bar and pouring temperature.

3.3.1 Measuring the Proportion of Strontium

The segregation behavior of strontium, discussed in Chapter 2, implied different concentration of strontium at the different areas of the specimens. Generally three areas were selected for each of the group #1 and group #2 samples, and five areas were selected on group #3 sample. All areas were located along the transversal radius. The area selected by EDS detector was 200μm x 200μm. An energy differential spectrometer (EDS) was utilized to obtain diagrams of strontium. Also, the distribution of strontium on the selected area could be determined by map scanning analysis. The distribution was associated with the solidifying pattern. Proper controlling of the solidification pattern would provide good samples for component analysis. Thus, FDA simulation combined with Flow-3D Casting was conducted to predict the flowing and solidifying pattern during the test.

3.3.2 Solidification Simulation

Commercial simulation software such as MAGMA software and Flow-3D Casting have been utilized for casting design and process optimization. Computation based on finite difference methods achieves high accuracy in predicting heat transfer and solidification during the casting process. Numerical simulation was used to predict the flow-solidify pattern and heat transfer with Flow-3D Casting. The results indicated the last solidifying area and temperature distribution in the casting.

A 3-D model was drafted with exactly the same dimension as the permanent mold used in the physical experiments. Melted alloys were poured from a ladle at 650℃. Melting alloys were set as A380 and initial parameters, such as viscosity, surface tension and heat transfer coefficient (HTC) that are associated with flowing and solidifying, were provided by the software. The temperature at the center of the test bar was set at 450℃. A schematic of the flow patterns used are shown n Figure 3.5.

During the pouring process, the melted fluid mode contact with the gating side (the pin side facing the ladle) firstly. Fluid was divided into two patterns and subsequently made contact with the mold wall. After contacting the mold wall, the flow front rebounded and filled the bottom part of the gating side. Simulation results of the flow pattern were consistent with the physical experiments' results. Because the asymmetric flow pattern involved disturbances in heat transferring, the temperature gradient during mold filling and solidification was also asymmetric. The mold was filled in 3.4 seconds and solidification started then.

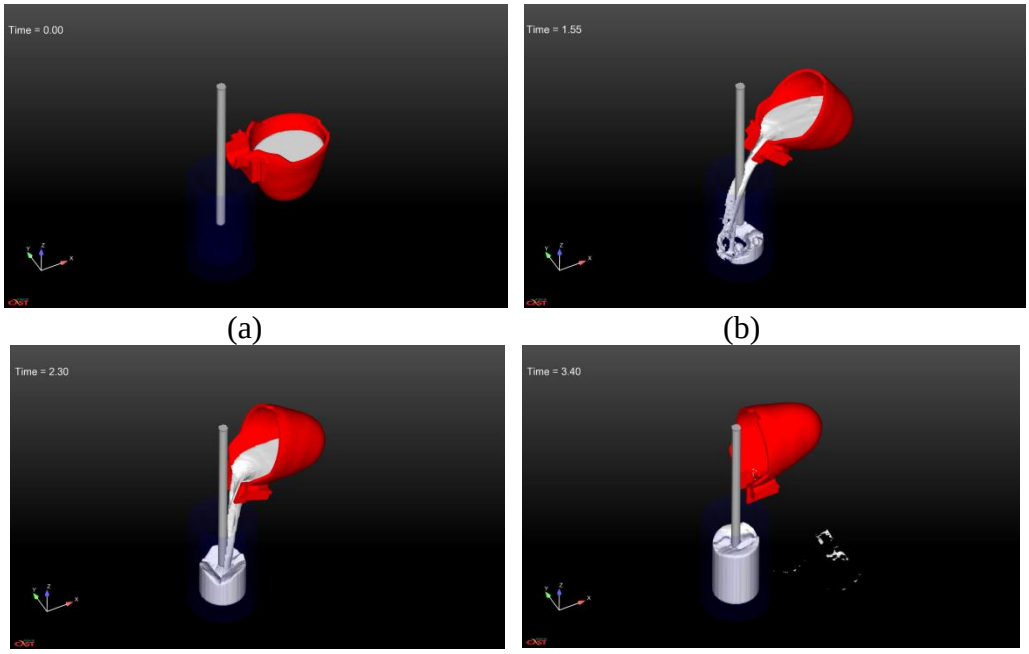

Figure 3.5 Flow Pattern

Solidifying pattern with temperature distribution is illustrated schematically in Figure 3.6. A 2D-Clip function in the Flow-3D Casting software is able to demonstrate the internal temperature field by providing sectional views of the 3D model. Solidification started from both the bottom and boundary regions where the temperature was the lowest. Shrinkage occurred around the core pin because the liquid there compensated for solidification shrinkage. Temperature distribution inside the casting is shown in Figure 3.6 (d). Both shrinkage and temperature were asymmetric relative to the core pin. The shrinkage at the gating side was stronger than the opposite site due to the asymmetric flow pattern. When the melting was poured into the mold, the liquid front made contact with the mold wall and rebounded to the other side. Temperature of the liquid dropped dramatically and solidification occurred at the right bottom area. This is verified in the next section by the presence of the second dendrite arm spacing.

Solidification shrinkage occurred due to different volumes of liquid and solid alloys. The process is demonstrated in Figure 3.6 (b).

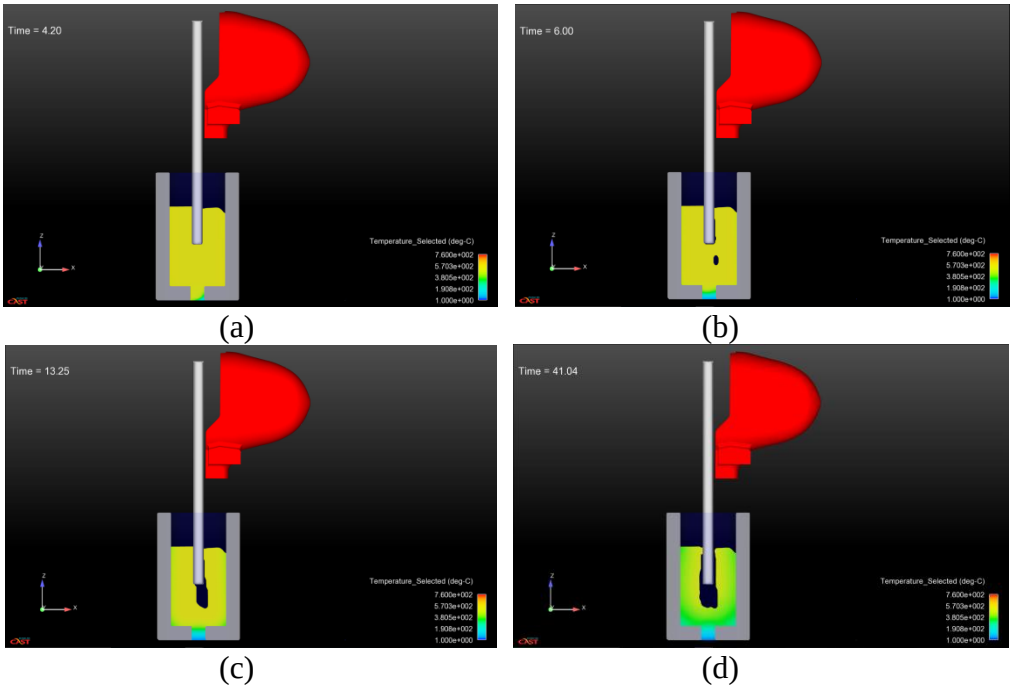

Figure 3.6 Solidify Pattern and Temperature Distribution

The areas near the mold wall were solidified after filling due to the low initial temperature of the mold wall. The compensating liquid for solidification shrinkage came from the center area because the core pin was preheated to 450℃ and the temperature drop rate was much lower than at the surroundings. Shrinkage finalized near the core pin. Shrinkage on the gating side was more severe than on the opposite side.

The simulation result was exaggerated compared to the physical experiment, in which actual shrinkage rate is normally 6% for aluminum alloys. However, the experiment accurately predicted the trend of flow and solidification. Specimens were made along the temperature gradient in Figure 3.6 (d) and solidification rates were determined by the presence of second dendrite arm spacing on the different areas.

3.3.3 Second Dendrite Arm Spacing

Second dendrite arms are responsible for insulating segregated phases into grain boundary or eutectic structure (R. N. Grugel, 1993). The segregation behavior of strontium was discussed in previous chapters. During the solidification process of A380, silicon eutectic is formed between the second dendrite arms and strontium is segregated on the boundary of the dendrite arms.

Second dendrite arm spacing, notated as λ_2, serves as an indication of cooling rate, which also implies growth velocity and temperature gradient. Previous researches by G. R. Kotler, et al illustrates that second dendrite arm space λ_2 and cooling rate V followed linear relationships. Directional solidification experiments have been conducted by R. N. Grugel with Al-Si alloys, in which the concentration of silicon ranged from 4-12 wt%. Figure 3.7 is a diagram of λ_2 as a function of cooling rate denoted by directional solidification experiments.

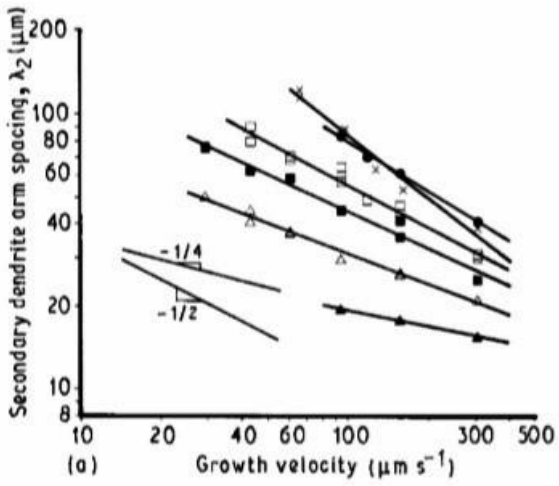

Figure 3.7 Second Dendrite Arm Spacing vs Growth Rate

The linear formula for second dendrite arm space was given by G. R. Kotler, et al as:

$$\lambda_{II} = KV^{-n}$$

where V is the growth rate; K is a proportionality constant based upon the initial composition of the casting alloy. Exponent n ranges from -0.32 to -1.1 depending on the composition of the alloys. Thus, cooling rate can be calculated by λ_2 given parameters K and n. Generally, a thinner second dendrite arm space indicates a higher cooling rate and a thicker second dendrite arm space indicates a lower cooling rate

3.4 Instrumentation

A mixture of A380 alloy and strontium at a constant temperature was required for the experiment. Thus, a casting system was required for melting and mixing the materials. Microstructures of the specimens were to be observed using an optical microscope as well as a scanning electron microscope. Also, distribution of strontium on different areas of the specimens was determined using an energy differential spectrometer and a backscattered electron function.

A thermo Scientific Lindberg/Blue M Moldatherm Box Furnace, shown in Figure 3.8, was used for melting the alloys and holding the temperature at a constant level. Temperatures could reach to 700℃ within two hours with 40% of output level. Figure 3.8 (a) shows the exterior of the furnace and Figure 3.8 (b) shows the interior of the furnace.

(a) (b)

Figure 3.8 Thermo Scientific Lindberg/Blue M Moldatherm Box Furnace

A LECO diamond saw shown in Figure 3.9 was used for cutting the samples.

Figure 3.9 LECO Diamond Saw

During the mold filling experiment, the temperature of the melt was measured using a thermocouple.

Preparation of samples was made using a Buehler electro-polish device as shown in Figure 3.10. The voltage was set to 20V and pump was set between 60% and 70%. Polishing time was 5 seconds. The composition of the solution used for electro-polishing is given in Table 3.2.

Table 3.2 Composition of Solution for Electro-Polishing

Materials	Distilled Water	Ethanol	Per-chloric Acid
Volume (mL)	140	800	60
Percentage	-	95%	70%

Figure 3.10 Buehler Electro-Polish Machines

A Leica Optical microscope was used for observing dendrites and eutectic structure. Microscope is shown in Figure 3.11. The magnification ranges from 50x to 500x were available.

Figure 3.11 Leica Optical Microscope

A scanning electron microscope (SEM) was used to investigate the microstructure of dendrite and eutectic structures in each specimen, while the components distribution was studied by an energy dispersive spectrometer (EDS). The SEM system is shown in Figure 3.12.The structure of intermetallic layers was studied using backscattered electron micrographs (BSE).

Figure 3.12 SEM system

3.5 Data Analysis

The microstructure photographs taken by optical microscope and scanning electron microscope were analyzed and compared in groups categorized by strontium concentration. Second dendrite arm spacing was calculated according to the scale in each photograph. Composition data along the radius of the specimens, obtained from energy differential spectrometer, was analyzed. A phase diagram was developedto illustrate the distribution of strontium in the specimens.

3.6 Standard of Success

The purpose of the research is to determine the effect of strontium on soldering resistance. Finding the segregation of strontium near the core pin with EDS would highly imply that a layer consisting of strontium is formed. On the other hand, if particles

containing high concentrations of strontium are found near the core pin, there is high possibility that strontium segregated around the core pin. If layers of strontium oxide or eutectic structure are found around the core pin, it is highly implied that the layers associated with strontium are responsible on soldering resistance. There statements collectively represent the standard of success for the study

3.7 Summary

This chapter discussed the methodology used in the experiment. The approaches for obtaining and preparing the specimens were developed. The data and instruments needed for the analysis were also clarified. Finally standard of success in the study was identified.

CHAPTER 4. EXPERIMENTAL RESULTS

This chapter presents the results of the experiment in a macro-analysis and micro-analysis format. Macro-analysis dealt with results of second dendrite arm spaces and the distribution of strontium and strontium particles along the radius. The magnification for macro-analysis ranged from 100x to 500x. Micro-analysis dealt with results from observation made using EDS and BSE on strontium particles and compositions. The magnification for micro-analysis ranged from 2000x to 5000x.

4.1 Determine Solidifying Direction

The microstructure of specimens was observed by means of an optimal microscope. Specimens were labeled from one to three in terms of the initial concentration of strontium. Also, two positions were sectioned and labeled as #1 and #2 on each sample to observe the difference in the dendrite arm space at different areas. The positions that were selected for observation are illustrated in Figure 4.1.

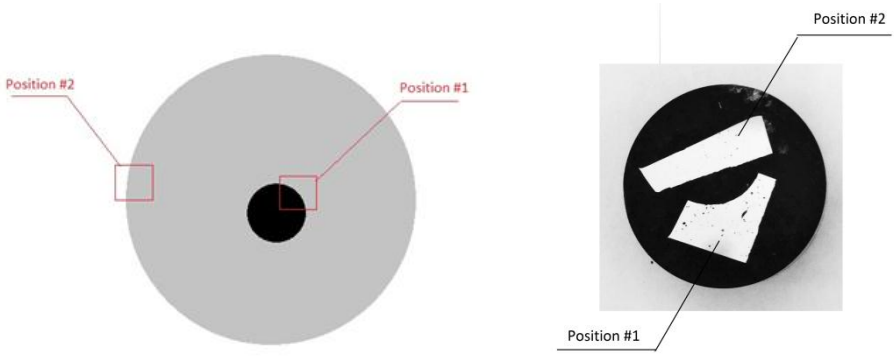

(a) (b)

Figure 4.1 Sample Positions

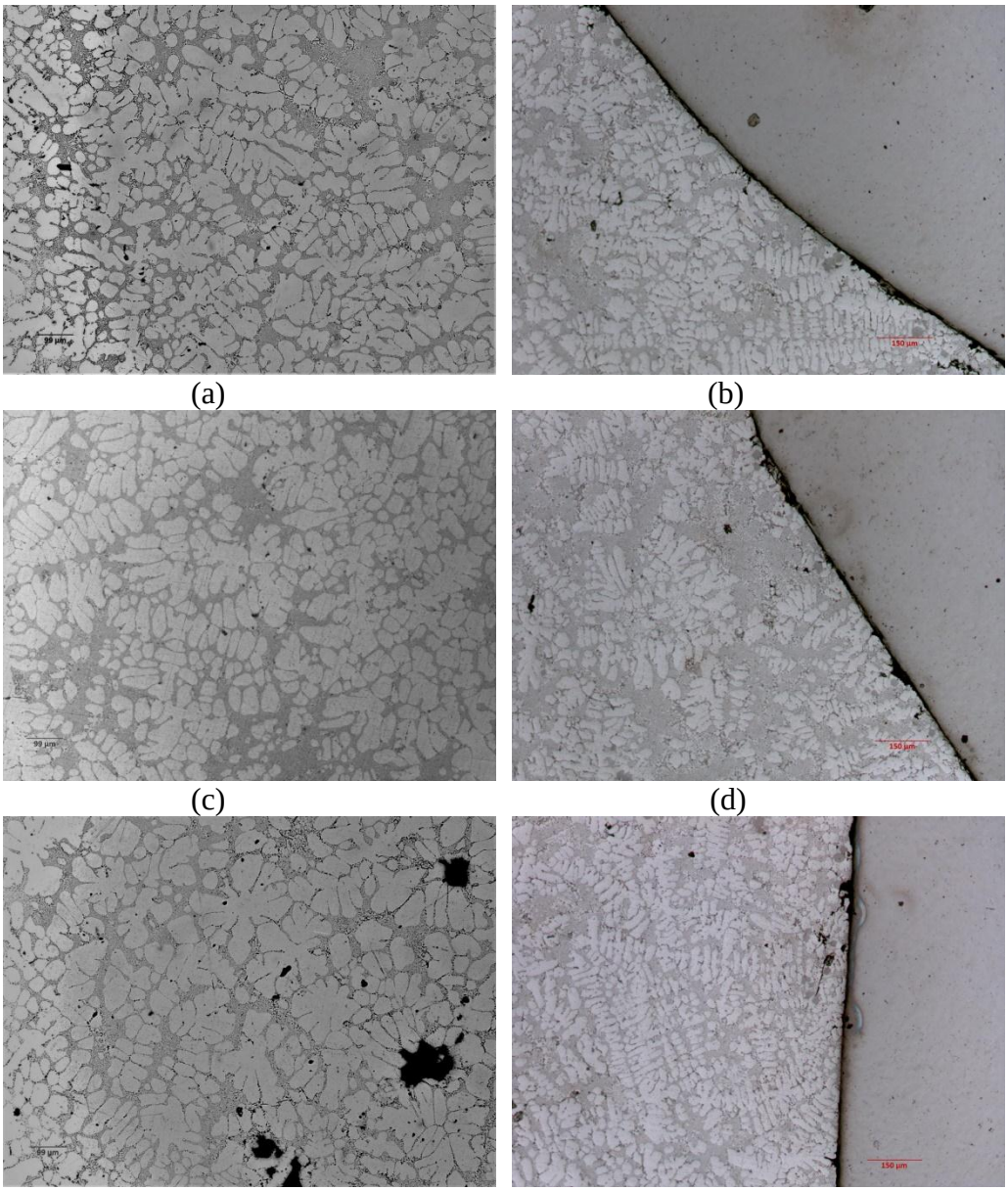

(a) (b)

(c) (d)

(e) (f)

Figure 4.2 Second Dendrite Arm Spacing

The transverse area of the sample is shown in Figure 4.1 (a). Two positions were selected and cut for making mounting specimens for microstructure observation. These are shown in Figure 4.1 (b). Position#1 is the core pin area where the cooling rate was expected to be the lowest. Position#2 is the boundary area where the cooling rate was

expected to be the highest. The second dendrite arm spaces of the two specimens were compared.

Microstructures of the two specimens were observed by optical microscope. Metallographic photographs of the specimens are shown in Figure 4.2. The magnification for the sample specimens is 100. Figure 4.2 (a) and Figure 4.2 (b) are microstructures of group#1, in which the concentration of strontium was 0.03%wt; Figure 4.2 (c) and Figure 4.2 (d) shows microstructures of group#2, in which the concentration of strontium was 0.05%; Figure 4.2 (e) and Figure 4.2 (f) are microstructures of group#3, in which the concentration of strontium was 0.07%wt. Figure 4.2 (a), Figure 4.2 (c) and Figure 4.2 (e) were taken at position #1 in each specimen; Figure 4.2 (b), Figure 4.2 (d) and Figure 4.2 (f) were taken at position #2 in each specimen. The scale of the photograph was 100μm shown at the bottom left corner.

Second dendrite arm spaces were defined using the term λ_{II}. The average λ_{II} is calculated and the result was shown in Table 4.1. The comparison of $\lambda_{II}a$, $\lambda_{II}c$, and $\lambda_{II}e$ value indicates that strontium level had an influence on the second dendrite arm spaces. Second dendrite arm spaces follow the older: $\lambda_{II}a < \lambda_{II}c < \lambda_{II}e$, indicating that a higher strontium level results in a larger second dendrite arm space. On the other hand, comparison between $\lambda_{II}a$ and $\lambda_{II}b$ (or $\lambda_{II}c$ and $\lambda_{II}d$ or $\lambda_{II}e$ and $\lambda_{II}f$) illustrates that second dendrite arm spaces in location #1 are significantly larger than in location#2. The theoretical statement in Chapter 3 illustrated a linear relationship between cooling rate and second dendrite arm space. A larger second dendrite arm space in location#1 indicates a lower cooling rate.

Table 4.1 Second Dendrite Arm Spaces in Different Specimens λ_{II} (μm)

Label	Area #1	Area #2	Area #3	Average
$\lambda_{II}a$	33.5	36.9	34.9	35.1
$\lambda_{II}b$	16.0	14.6	17.5	16.0
$\lambda_{II}c$	37.4	37.8	34.9	36.7
$\lambda_{II}d$	21.2	20.4	18.3	20.0
$\lambda_{II}e$	39.3	34.9	40.8	38.3
$\lambda_{II}f$	17.5	14.1	19.4	17.0

As previously mentioned, the test bar was preheated to 700℃ before pouring. Then,, the bar was inserted into the middle of the permanent mold. The temperature dropped dramatically due to rapid heat loss because the permanent mold remained at room temperature while the test bar made contact with the cooler mold and air. As the melted alloy was poured into the mold, the temperature of the test bar dropped below the solidus temperature of the alloys. During the mold filling, melted alloy contacted the bar and reheated it. During the solidification, the initial temperature of the test bar was much higher than the initial temperature of the mold wall, which was at room temperature. This resulted in a lower solidifying rate near the test bar than that near the mold wall.

4.2 Eutectic Structure

The morphology and proportion of eutectic structures that isolated into the dendrite arms consist were studied.

Optical morphologies of the eutectic structure are illustrated in Figure 4.3. The initial concentrations of strontium were 0.03%wt, 0.05%wt, and 0.07%wt.

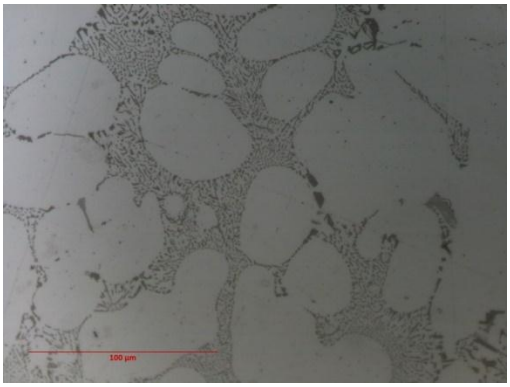

(a) 0.03%wt

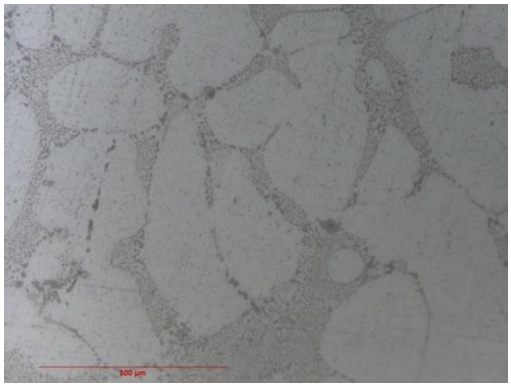

(b) 0.05%wt

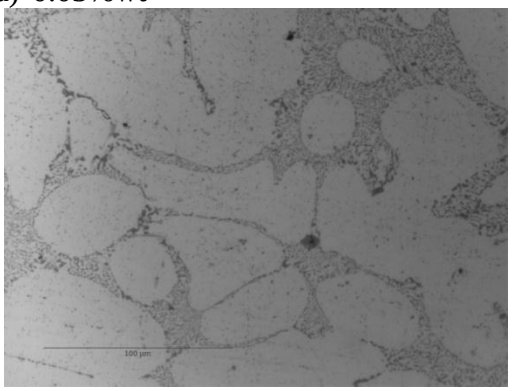

(c) 0.07%wt

Figure 4.3 Silicon Particles

Silicon eutectics were modified to fine and round particles. The areas selected in Figure 4.3 are eutectic structures in three groups in position#1. The initial needle-like silicon eutectic was modified to a round morphology, which increased the impact strength and ductility of the modified alloys.

Figure 4.3 (a) is the microstructure of group#1; Figure 4.3 (b) is the microstructure of group#2; Figure 4.3 (c) is the microstructure of group#3. Eutectic structures were segregated around the dendrite arms. Faceted silicon particles can still be observed in Figure 4.4 (a) implying that the modifying level of strontium on eutectic is not high enough to achieve total modification. In Figure 4.4 (b) and Figure 4.4 (c),

faceted silicon particles were all displaced by fine and round eutectic structure. The presence of strontium eliminated the initial orientation of eutectic growth and resulted in independently inter-dendritic growth.

Also, the eutectic grain size in group#3 is larger than in group#2 and group#1. This can be explained through nucleation and grain growth mechanism. The required level of strontium additive in modifying the eutectic structure was too low to cause significant change in the eutectic composition of Al-Si system according to the phase diagrams of Al-Sr and Si-Sr shown in previous chapter. Instead, strontium was only responsible for forming lattice defects and decreased the nucleation density of eutectic grains. This resulted in increasing of the grain size.

Despite the modified eutectic, diamond-shaped particles were found in Figure 4.3 (b) and Figure 4.3 (c). The areas circled in Figure 4.4 specify the characteristic morphology of the particles. The radial dimension of the particles ranges from 5μm to 15μm. The global distribution and dimension of the particles were studied by checking different areas on specimens using the SEM. Diamond-shaped particles appeared in both location#1 and location#2. However, the geometrical sizes of the particles in location#1 were larger than those in location#2. Also the density of the particles in location#1 was higher compared with location#2. Furthermore, no diamond-shaped particles were found in the 0.03%wt strontium specimens.

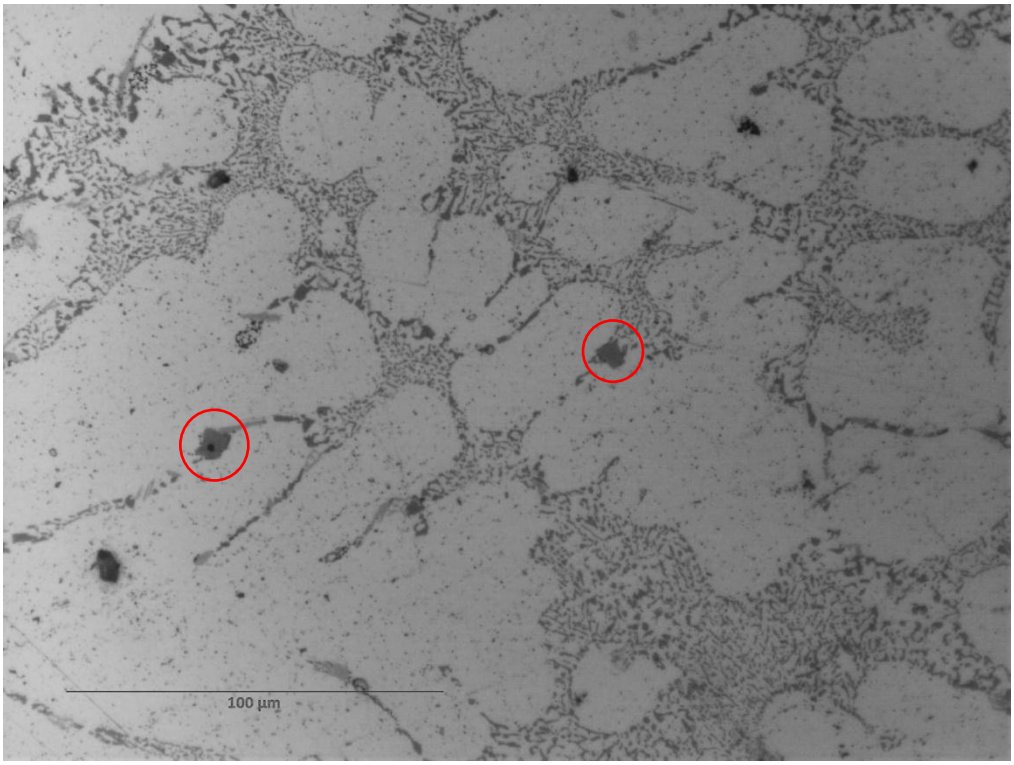

Figure 4.4 Diamond-Shaped Particles

Detailed microstructures were obtained from SEM photographs. The magnifications were 500x and 2000x. The photographs are shown in Figure 4.5. Figure 4.5 (a) and Figure 4.5 (c) shows the microstructures of group#2 in position#1 and Figure 4.5 (b) and Figure 4.5 (d) shows the microstructures of group#3 in position#1. Figure 4.5 (e) shows the microstructure of the specimen with 0.07%wt strontium in position#2. The particles were characterized by a regular diamond shape and were highlighted with high contrast. The particles were segregated on the eutectic structure and the diagonal length was found to range from 5µm to 10µm.

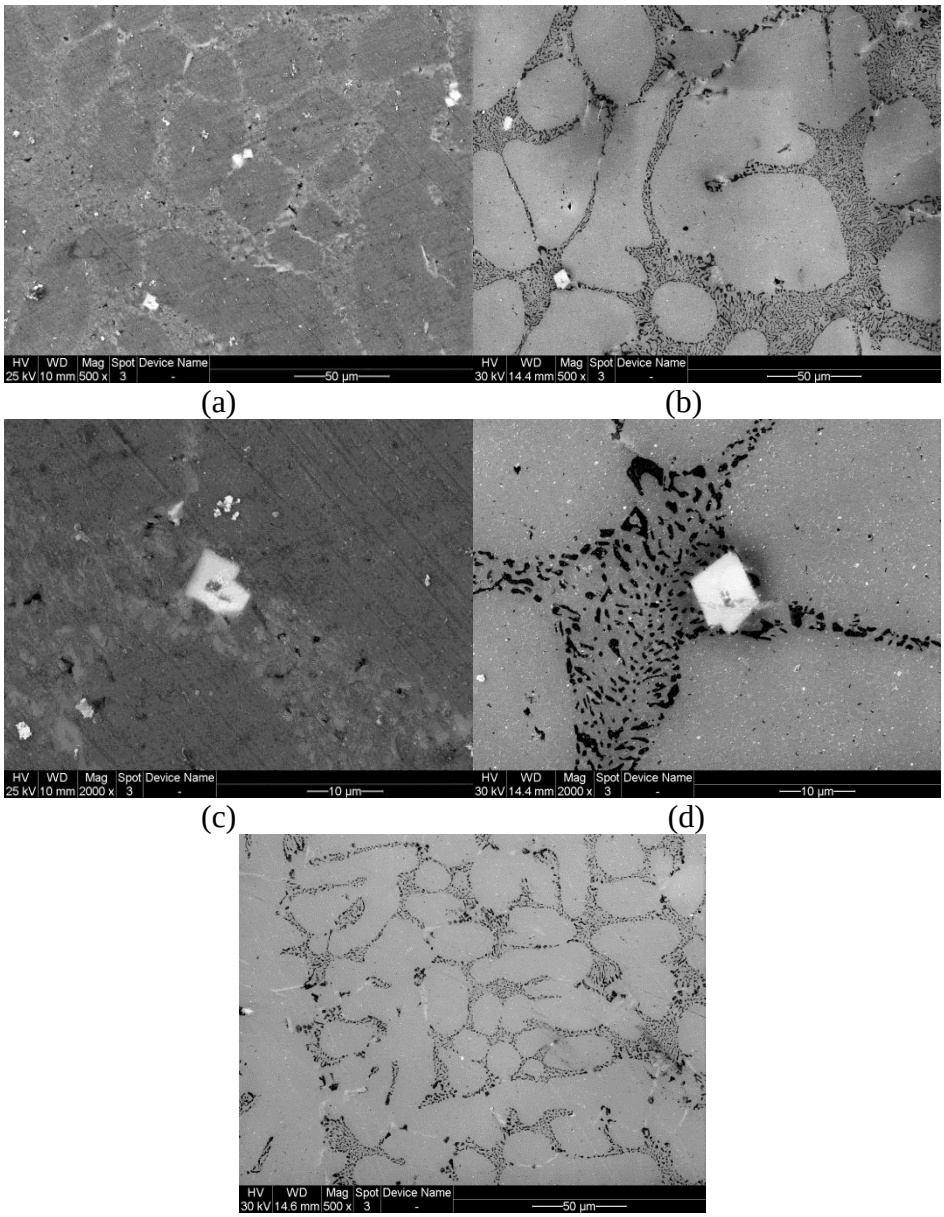

Figure 4.5 SEM Photographs of Diamond-Shaped Particles

The particles consistently appear to have regular geometry and were segregated at the eutectic structure. There could be high possibility that the particles are made up from a specific phase consisting of aluminum silicon and strontium.

4.3 Strontium Distribution

Morphologies of dendrite and eutectic were observed using an optical microscope and scanning electron microscope. Energy Differential Spectrometer was used to obtain the distribution and composition of the particles and to locate desired spots for study. Backscattered electron function was also used to observe the structure of strontium particles and iron particles. BSE was also used to verify the existence of strontium oxide layers.

4.3.1 Composition of Diamond-Shaped Particles

The compositions of the diamond-shaped particles were studied by EDS. Three particles were randomly selected from group#2 and group#3. Point scanning and selected area scanning were used to obtain accurate results. The voltage utilized was 30kV and the magnification was 500. Similar results in compositions of the particles were obtained by EDS. Results of component peaks are shown in Figure 4.6.

The compositions of diamond-shaped particles are illustrated in Figure 4.6. Three particles were randomly selected from specimens. Aluminum, silicon, and strontium were detected as characteristic peaks. Images for EDS were collected by secondary electron in SEM with 500x magnification. Aluminum and silicon peaks were detected in the initial composition of A380 alloys.

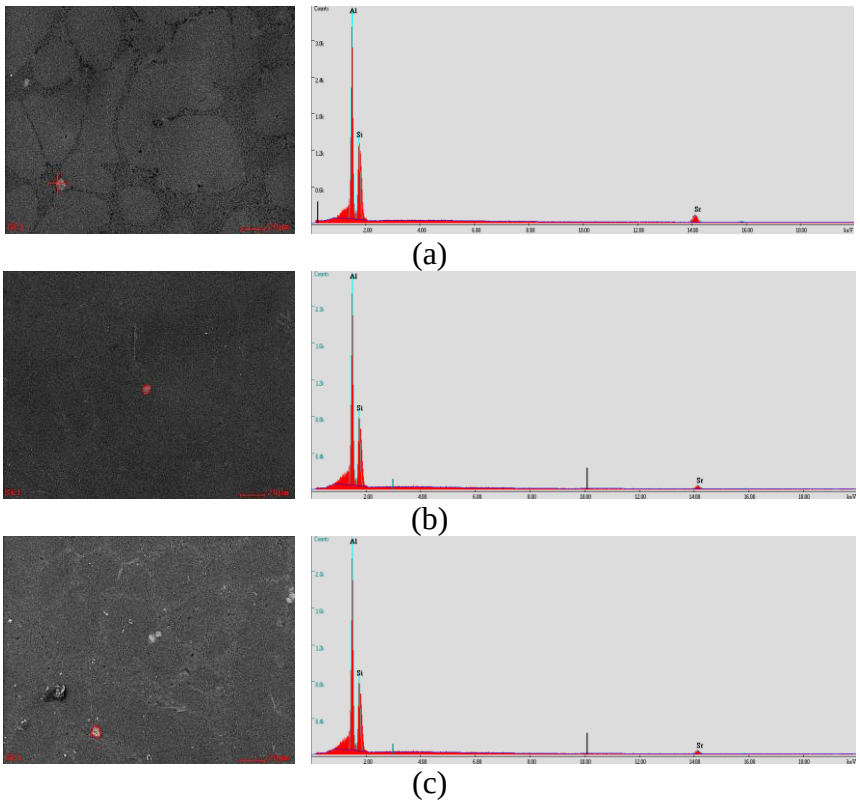

Figure 4.5 Compositions of Diamond-Shaped Particles

A strontium peak was found at 14.14kV in each result indicating that strontium was contained in the diamond-shaped particles. The quantitative results are illustrated in Table 4.2.

The quantitative results of weight percentages, denoted as Wt%, and atomic (or mole) percentages, denoted as At%, of aluminum silicon and strontium in the particles was given in the table. Average percentages were calculated. The atomic ratio between aluminum, silicon and strontium of the particles followed: 46:37:19. The chemical formula can be determined according to Table 2.1 in chapter two.

Table 4.2 Quantitative Data of Composition

Element	Wt%	At%
Al_a	34.68	47.27
Si_a	28.44	37.25
Sr_a	36.88	15.48
Al_b	29.18	41.40
Si_b	29.41	40.26
Sr_b	41.41	18.04
Al_c	35.76	49.46
Si_c	25.69	34.13
Sr_c	38.55	16.41
$Al_{average}$	33.21	46.04
$Si_{average}$	27.85	37.21
$Sr_{average}$	38.95	19.02

Three phases in Table 4.4 were selected from Table 2.1 in Chapter 2. There have the lowest enthalpies according to thermo calculation. The negative calculated enthalpies indicate that the phases are energetically steady. Ground state of the Al-Si-Sr intermetallic would be the phases with the lowest enthalpy. Thus, the AlSiSr and $Al_2Si_2Sr_3$ phases, listed in Table 4.3, are likely to be the ground state of the system. The atomic ratio of Al-Si-Sr was 4.6: 3.7: 1.9, which is close to the ratio 2: 2: 1. Thus, the chemical formula of the particle was written as Al_2Si_2Sr. The calculated enthalpy of the

particle is approximately -31kJ/mol and it can be formed easily and early during solidification.

Table 4.3 Al-Si-Sr Ternary Intermetallic

Phase	ΔH_f^{LDA}	ΔH_f^{GGA}	Cell Parameters		
			Expected Value		
			a	b	c
AlSiSr	-40.85	-43.43	4.23	4.23	4.74
Al_2Si_2Sr	-31.00	-31.38	4.18	4.18	7.41
$Al_2Si_2Sr_3$	-42.05	-43.34	4.07	4.82	19.00

Results of the line scanning are shown in Figure 4.7. The selected line is shown in white. The red line indicates the concentration of aluminum; the green line indicates the concentration of silicon; and the blue line indicates the concentration of strontium along the selected line. The level of strontium was much higher in Al_2Si_2Sr particles than in the surroundings. Thus, the presence of Al_2Si_2Sr particles implies the presence of strontium. Therefore, most of the strontium was segregated at the boundary of the dendrite and formed the Al_2Si_2Sr particle in the eutectic structure.

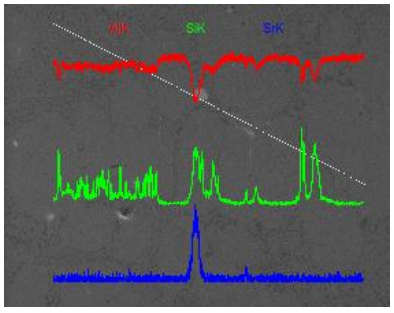

Figure 4.7 Line Scanning of Al_2Si_2Sr Particles and Eutectic

4.3.2 Cross Section of Soldering Area

The cross section of the soldering area on the samples were studied using the SEM. The microstructure of the soldering areas was observed by the SEM and composition was analyzed by the EDS. Photographs of the SEM observation are shown in Figure 4.8.

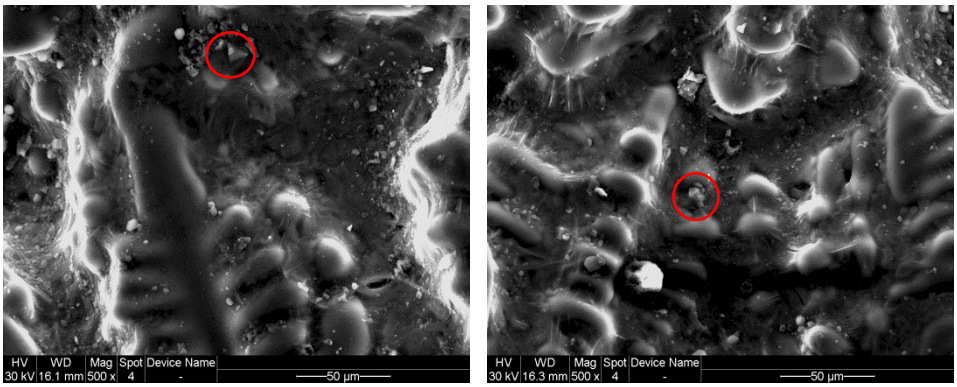

(a) (b)

Figure 4.8 Cross Section of Soldering Areas

Outlines of primary dendrite and secondary dendrite arms are clearly shown in Figure 4.8 (a). Based on the scale illustrated at the bottom of the figure, the second dendrite arm space is approximately 35µm. Small particles, circled in the Figure 4.8, were segregated around the dendrite arms. The composition of the particles was detected using the EDS.

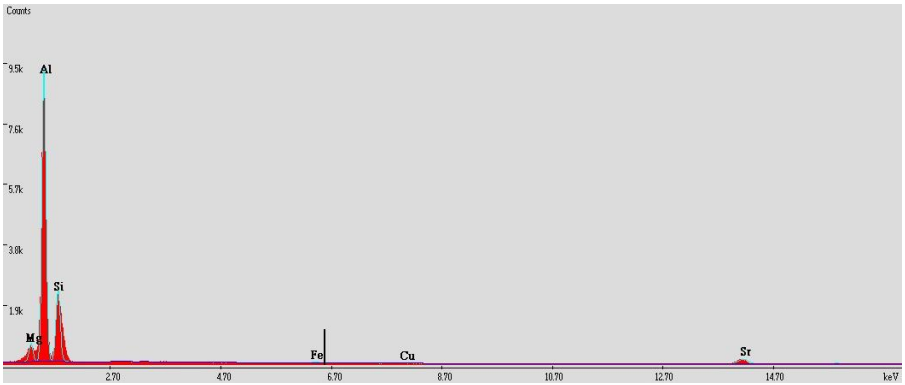

Figure 4.9 Compositions of Selected Particles

Figure 4.9 shows the composition of the selected particles in Figure 4.8. The quantitative proportion of each element is shown in Table 4.4.

Table 4.4 Compositions of Selected Particles

Element	Al	Si	Sr	Other
Wt%	45.28	26.21	24.80	3.70
At%	55.36	30.79	9.34	4.51

The characteristic element peaks of the particles consist of aluminum, silicon and strontium. The morphology of the particles also has a regular geometry. Thus, the particles are the Al-Si-Sr ternary phase, and most likely to be Al_2Si_2Sr due to the composition error by EDS. Also, the concentration of iron around the particles was zero based on the results from the EDS.

On the other hand, global concentrations of strontium on the cross sections were detected using the EDS and illustrated in Table 4.5. The primary element peaks were aluminum silicon. The concentration of strontium is 0.23%wt. Concentration of strontium on the cross section was much higher than the initial concentration of strontium of 0.07% in group#3. Thus, strontium was segregated at the cross section of the soldering areas.

Table 4.5 Global Composition of Cross Section Area

Element	Al	Si	Sr	Other
Wt%	79.78	15.25	0.23	4.84
At%	83.27	15.26	0.10	1.43

4.3.3 Detection of Strontium Oxide Layer on Soldering Areas

Soldering areas were selected from group#2 and group#3 in which the concentration of strontium was 0.05% and 0.07%. Multiple spots were selected from the soldering areas for composition analysis. The backscattered electron photographs of group#2 are shown in Figure 4.10 (a) and Figure 4.10 (b). The magnification was 5000x. Highlighted spots in the BSE photographs indicate particles with high atomic numbers. Compositions of the particles were analyzed using EDS.

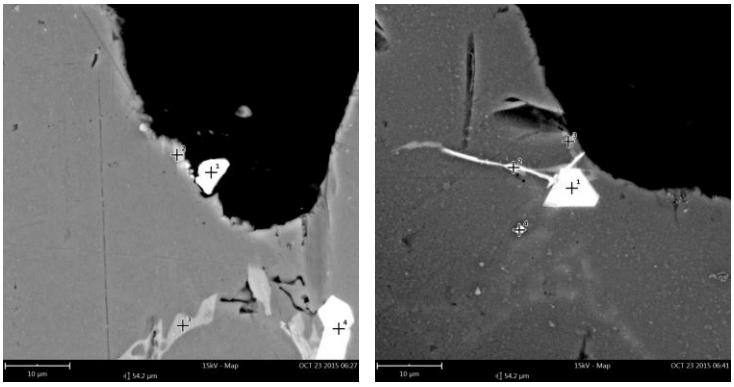

(a) (b)

Figure 4.10 Backscattered Electron Photographs on Soldering Areas in Group#2

The spectrums of selected spots are shown in Figure 4.11. Figure 4.11 (a) to Figure 4.11 (d) show the spectrums of spot 1 to spot 4 in Figure 4.10 (a); Figure 4.11 (e) and Figure 4.11 (h) are spectrums of spot 1 and spot 2 in Figure 4.10(b). Strontium was found in all selected spots in Figure 4.10 (a) and in spot 1 in Figure 4.10 (b). Iron was found in spot 2 in Figure 4.10 (b) and no iron was found in Figure 4.10 (a). The quantitative compositions of the selected points are given in Table 4.7.

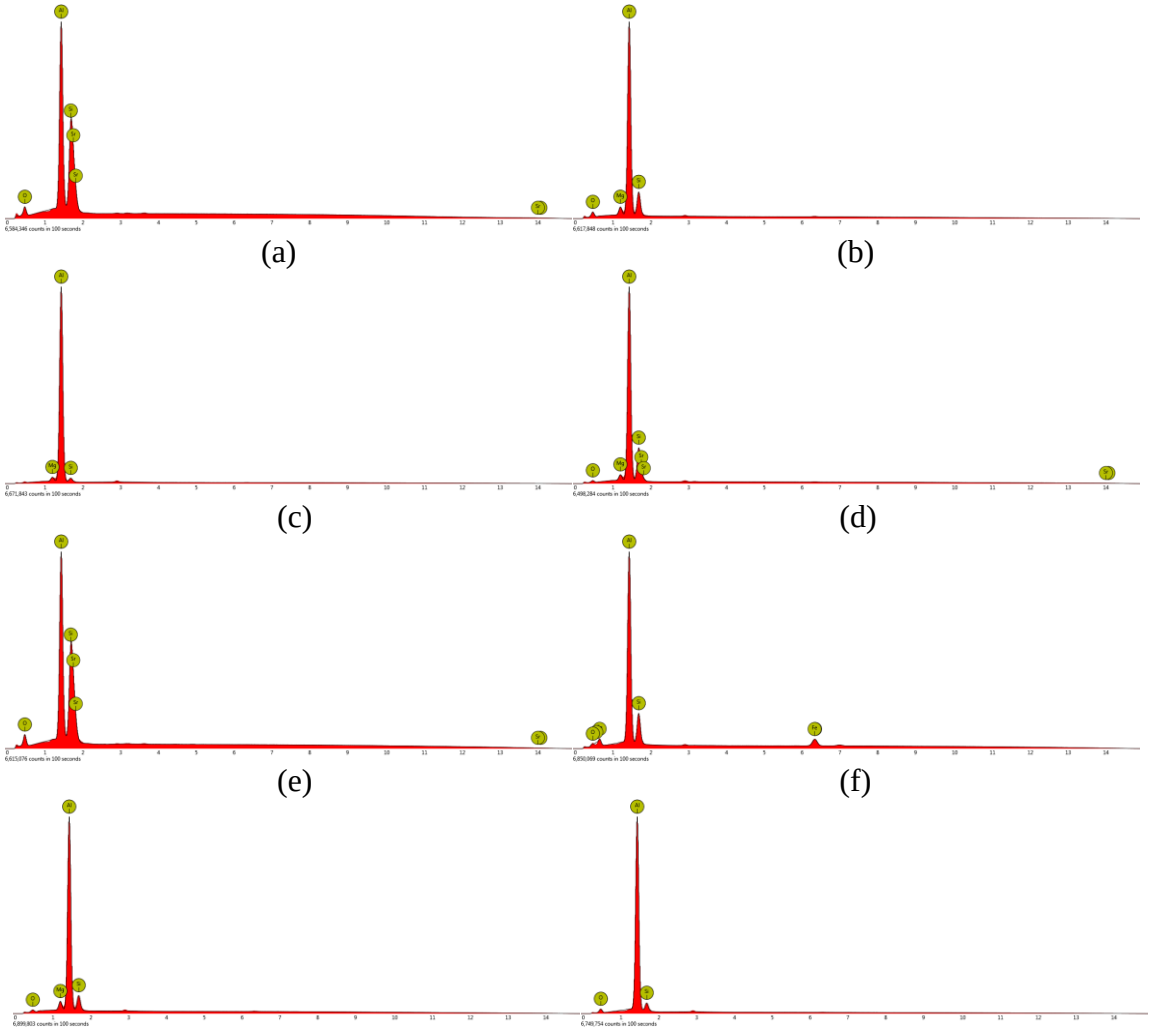

(a) (b)

(c) (d)

(e) (f)

(g) (h)

Figure 4.11 Spectrums of Selected Spots in Group#2

The quantitative compositions of selected spots are listed in Table 4.6. Spot 1 in Figure 4.10 (a) refers to a particle consisting of strontium and oxygen. Thus, indicating a strong likelihood that the particle was an oxide of Al-Si-Sr or Al-Sr depending on the formation enthalpy. Also, the morphology of the particle is irregular and a small gap appears between the particle and the aluminum. An interesting item worth mentioning in the fact was that the concentration of iron around the strontium particle was absolutely zero. Therefore, one can assume that the particles were a part of the oxide layers

consisting of strontium. The oxide layer was prevented the iron from diffusing into the aluminum. However, the layer peeled off during ejection or the mounting process.

Table 4.6 Quantitative Composition of Selected Spots At%

Element	Al	Si	Sr	Fe	O	Other
(a)	42.3	25.4	9.0	0	23.2	0.1
(b)	71.9	64.4	16.3	0	16.0	3.3
(c)	64.1	92.8	4.9	0	-	2.3
(d)	66.4	22.6	1.9	0	6.6	2.5
(e)	39.3	24.3	8.8	0	27.6	0
(f)	67.5	20.1	0	6.5	5.9	0
(g)	74.9	13.4	0	0	7.6	4.1
(h)	76.8	7.6	-	0	15.6	-

Spot 2 and spot 3 in Figure 4.11 (a) are a eutectic structure. Spot 2 in Figure 4.10 (b) is a needle-like iron particle. Spot 4 in Figure 4.10 (a) and spot 1 in Figure 4.10 (b) are Al_2Si_2Sr particles characterized by the diamond-shaped morphology.

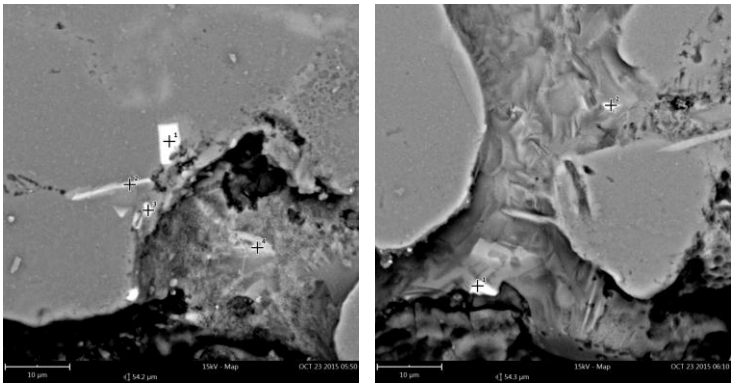

(a) (b)

Figure 4.12 Backscattered Electron Photographs on Soldering Areas of Group#3

Figure 12 shows BSE photographs on soldering area in Group #3. The spectrums of selected points in Figure 4.12 are shown in Figure 4.13. Figure 4.13 (a) to Figure 4.13 (d) are spectrums of spot 1 to spot 4 in Figure 4.12 (a); Figure 4.13 (e) and Figure 4.13 (f) are spectrums of spot 1 and spot 2 in Figure 4.12(b). Strontium was found in spot 1 and spot 3 in Figure 4.12 (a) and spot 1 and spot 2 in Figure 4.12 (b). Iron was found in all spot expect spot 1 in Figure 4.12 (a). The quantitative compositions of selected points are given in Table 4.7.

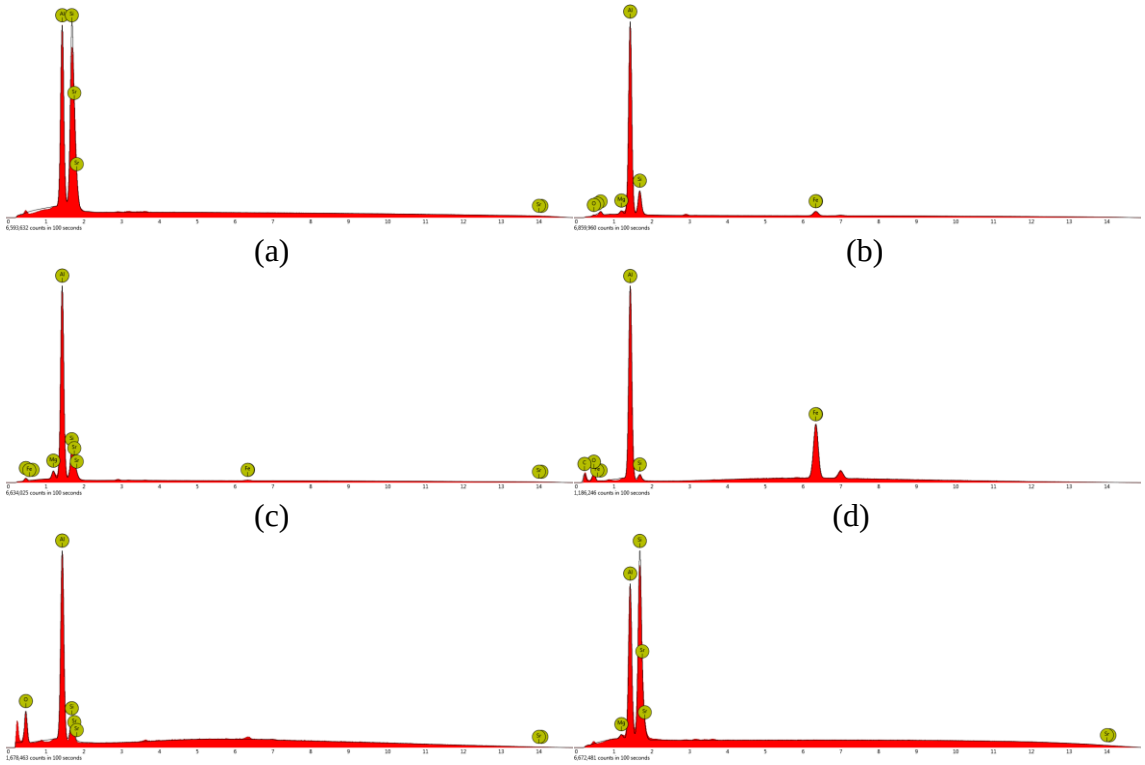

Figure 4.13 Spectrums of Selected Spots in Group#3.

The composition and geometric character of spot 1 indicates that the spot is an Al_2Si_2Sr particle. Spot 2 and spot 4 in Figure 4.13 (a) are particles enriched with iron. The concentration of iron is inaccurate because the particles are too small and backscattered electron microscope cannot concentrate exactly on the center of the

particles. The iron particles have the needle-like shape and are distributed around the strontium particles.

Table 4.7 Quantitative Composition of Selected Spots At%

Element	Al	Si	Sr	Fe	O	Other
(a)	38.8	34.9	12.9	0	13.3	0.1
(b)	71.9	17.9	0	4.7	3.8	1.7
(c)	64.1	16.3	5.3	0.6	10.2	3.5
(d)	54.7	1.8	0	27.0	12.6	3.9
(e)	41.2	7.4	0.4	3.9	45.2	1.9
(f)	35.8	57.8	5.0	1.3	-	-

Based on the results from group#3, some interesting findings can be presented. First, the iron particles have the needle-like morphology and stretch along the eutectic structure. Second, the iron particles initiate from strontium particles and extend into the surrounding region in a certain orientation. Third, the proportion of strontium in the particles is zero. Thus, there is high possibility that strontium particles entrapped surrounding iron atoms and the iron particles were nucleated on the strontium particles. The entrapment of iron prevents the diffusion of iron into aluminum.

4.4 Summary

Chapter Four analyzed the microstructure and composition of the specimens. The morphology of eutectic structure and silicon particles was illustrated in this chapter. Also, the distribution of strontium along the radius of the specimens was also discussed.

CHAPTER 5 CONCLUSIONS AND FUTURE WORK

5.1 Discussion

Before dealing with the conclusion for the study, a discussion of two important topics is presented. Two arguments were proposed by the author to illustrate the effect of strontium on soldering resistance. There are: (1) the precipitation of strontium particles is concerned with nucleation of iron particles and (2) the effect of strontium oxide layers will be discussed. All the results from the experiments are repeatable.

5.1.1 Discussion of Strontium Particles on Nucleation

Al_2Si_2Sr particles were found in the eutectic structure. Previous simulation using ThermoCalc software with TTAL4 database indicated that Al_2Si_2Sr was formed at an early stage of solidification (J. Hirsch, 2008).

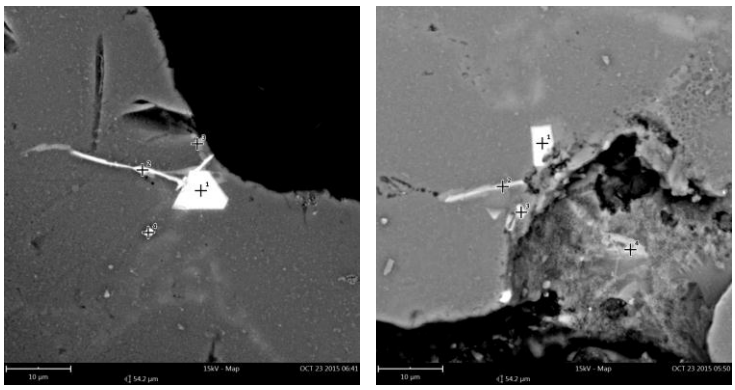

(a) (b)

Figure 5.1 Strontium Particles and Iron particles

The formation of Al_2Si_2Sr created an intermetallic layer around the nucleating agent and significantly decreased the nucleation of eutectic and the β-Al_5FeSi needle-like

phase. Increasing the level of strontium also melted in an increase in the proportion of Al_2Si_2Sr particles.

On the other hand, strontium particles, likely to be Al_2Si_2Sr, decrease the formation of Al-Fe intermetallics by capturing the nucleating agent. The formation of the Al-Fe intermetallics is a critical step for forming the soldering layer. BSE investigation indicated that the diffused iron atoms were captured by the strontium particles, as shown in Figure 5.1. Needle-like iron particles nucleated on the strontium particles with the participation of aluminum and silicon and grew along the eutectic structure. Thus, it can be proposed that strontium particles attracted iron atoms and served as nucleating agent for iron particles. The surroundings of the strontium particle were enriched with iron atoms and poor in aluminum. Therefore, the precipitation of strontium particles suppressed the diffusion of iron into the aluminum and also the diffusion of aluminum into iron.

5.1.2 Discussion of Formation of Strontium Oxide

Oxide consisting of aluminum and strontium was found on the soldering areas.

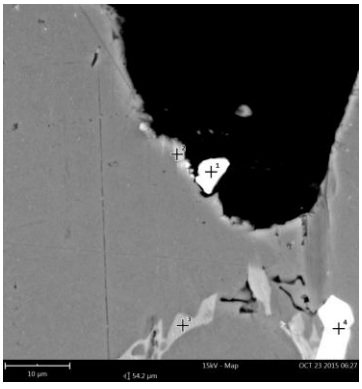

Figure 5.2 Al-Sr Oxide

The morphology of the remaining oxide is shown in Figure 5.2. Previous study by

Habibi illustrated that Al_2SrO3 formed much easier than aluminum oxide during the melting process. The composition of oxide measured by EDS was consistent with Habibi's research. The concentration of iron around the oxide was absolutely zero based on the results from the EDS study on the selected area. Therefore, a proposal was made that a continuous oxide layer consisting of Al_2SrO_2 was formed during solidification at the soldering area. The measured thickness of the oxide layer ranged from 3µm to 6µm. Also, the layer effectively prevented the diffusion between iron and aluminum. Therefore, the soldering activity was restricted. However, the adherion force of the oxide layer to the aluminum casting was relatively low and the layer was peeled off during ejection and mounting process.

5.2 Conclusions

The outcome of the research provided two proposals involving the effect of strontium on soldering resistance and verified the segregation of strontium for a casting undergoing thermal change.

The study shows that, strontium particles absorb iron atoms and act as a nucleating agent for iron particles. The precipitation of strontium particles decrease the level of aluminum and increase the level of iron on the areas where soldering is going to occur. Thus, the diffusion between aluminum and iron is significantly suppressed. Therefore, formation of Al-Fe intermetallic is suppressed and the soldering reaction is stopped.

Also, an oxide layer consisting of aluminum and strontium is formed at the early stage of solidification. The layer acts as a physical barrier and restricts the diffusion

between iron and aluminum. Thus, the soldering reaction is stopped as the layer is formed.

Finally, the distribution of strontium particle implied that the strontium was segregated into the eutectic along the grain boundary. Segregation followed the solidifying direction wherein the density of strontium particles in center areas was larger than that in the boundary areas.

5.3 Future Work

Due to the limitation of research time, only qualitative analyses to illustrate the effect of strontium on soldering resistance were conducted. Two proposals were made; however, further study is required for verifying the proposals.

Because the initial concentration of strontium only ranged from 0.03%wt to 0.07%wt, it is recommended that samples with higher concentration of strontium need to be examined to achieve the extreme condition for soldering resistance. Also, the pouring temperature in the research ranged from 650℃ to 665℃. Thus, it is recommended that a larger range of temperature should be used to investigate the temperature of forming the Al_2Si_2Sr and Al-Sr oxide layers.

Finally, the relationship of growth orientation between the strontium particle and iron should be investigated to verify the two proposals.

LIST OF REFERENCES

LIST OF REFERENCES

Chen, Z. W. (2005). Formation and progression of die soldering during high pressure die casting. *Materials Science and Engineering: A*, *397*(1), 356-369.

Clapham, L., & Smith, R. W. (1988). Segregation behaviour of strontium in modified and unmodified Al-Si alloys. *Journal of Crystal Growth*, 92(1), 263-270.

Dahle, A. K., Nogita, K., McDonald, S. D., Zindel, J. W., & Hogan, L. M. (2001). Eutectic nucleation and growth in hypoeutectic Al-Si alloys at different strontium levels. *Metallurgical and Materials Transactions A*, 32(4), 949-960.

Doremus, R. H., Roberts, B. W., & Turnbull, D. (1958). Growth and perfection of crystals.

Garay-Tapia, A. M., Romero, A. H., Trapaga, G., & Arróyave, R. (2012). First-principles investigation of the Al–Si–Sr ternary system: Ground state determination and mechanical properties. *Intermetallics*, 21(1), 31-44.

Glicksman, M. E. (2010). Principles of solidification: an introduction to modern casting and crystal growth concepts. *Springer Science & Business Media*.

Grugel, R. N. (1993). Secondary and tertiary dendrite arm spacing relationships in directionally solidified Al-Si alloys. *Journal of materials science*, 28(3), 677-683.

Han, Q., & Viswanathan, S. (2003). Analysis of the mechanism of die soldering in aluminum die casting. *Metallurgical and Materials Transactions A*, 34(1), 139-146.

Jackson, K. A. (1958). *Liquid metals and solidification*. *ASM*, Cleveland, 174.

Kaufman, J. G., & Rooy, E. L. (2004). Aluminum alloy castings: properties, processes, and applications. *Asm International*, 6(1), 35-43.

Khan, F. F., Bae, G., Kang, K., Kumar, S., Jeong, T., & Lee, C. (2009). Development of cermet coatings by kinetic spray technology for the application of die-soldering and erosion resistance. *Surface and Coatings Technology*, 204(3), 345-352.

Kopper, A., & Donahue, R. J. (2006). Soldering resistance mechanisms of novel Al-Sr-Si die casting alloys. The Minerals, Metals & Materials Society, 6(1), 801-805.

Kattner, U. R. (1997). The thermodynamic modeling of multicomponent phase equilibrium. *JOM*, 49(12), 14-19.

Kim, K. J., Kim, H. J., & Jeong, C. Y. (2014). Mechanical and die soldering properties of Al-Si-Mg-Mn cast alloy. *Materials Research Innovations*, 18(S2), S2-666.

Liu, L., Samuel, A. M., Samuel, F. H., Doty, H. W., & Valtierra, S. (2004). Characteristics of α-dendritic and eutectic structures in Sr-treated Al—Si casting alloys. *Journal of materials science*, 39(1), 215-224.

Murray, J. L., & McAlister, A. J. (1984). The Al-Si (aluminum-silicon) system. *Bulletin of Alloy Phase Diagrams*, 5(1), 74-84.

Nazari, K. A., & Shabestari, S. G. (2009). Effect of micro alloying elements on the interfacial reactions between molten aluminum alloy and tool steel.Journal of Alloys and Compounds, 478(1), 523-530.

Nogita, K., Yasuda, H., Yoshida, K., Uesugi, K., Takeuchi, A., Suzuki, Y., & Dahle, A. K. (2006). Determination of strontium segregation in modified hypoeutectic Al–Si alloy by micro X-ray fluorescence analysis. *Scripta material*, 55(9), 787-790.

Sadiq, M., & Lindsay, W. L. (1979). Selection of standard free energies of formation for use in soil chemistry. Technical bulletin-Colorado State University, Agricultural Experiment Station (USA).

Shabestari, S. G., Keshavarz, M., & Hejazi, M. M. (2009). Effect of strontium on the kinetics of formation and segregation of intermetallic compounds in A380 aluminum alloy. *Journal of Alloys and Compounds*, 477(1), 892-899.

Shankar, S., & Apelian, D. (2002). Die soldering: Mechanism of the interface reaction between molten aluminum alloy and tool steel. *Metallurgical and Materials Transactions B*, 33(3), 465-476.

Shankar, S., Riddle, Y. W., & Makhlouf, M. M. (2004). Nucleation mechanism of the eutectic phases in aluminum–silicon hypoeutectic alloys. *Acta Material*, 52(15), 4447-4460.

Timpel, M., Wanderka, N., Schlesiger, R., Yamamoto, T., Lazarev, N., Isheim, & Banhart, J. (2012). The role of strontium in modifying aluminium–silicon alloys. *Acta Material*, 60(9), 3920-3928.

Zhu, H., Guo, J., & Jia, J. (2002). Experimental study and theoretical analysis on die soldering in aluminum die casting. *Journal of materials processing technology*, 123(2), 229-235.

Zolotorevsky, V. S., Belov, N. A., & Glazoff, M. V. (2010). Casting aluminum alloys. Elsevier.

APPENDIX

APPENDIX

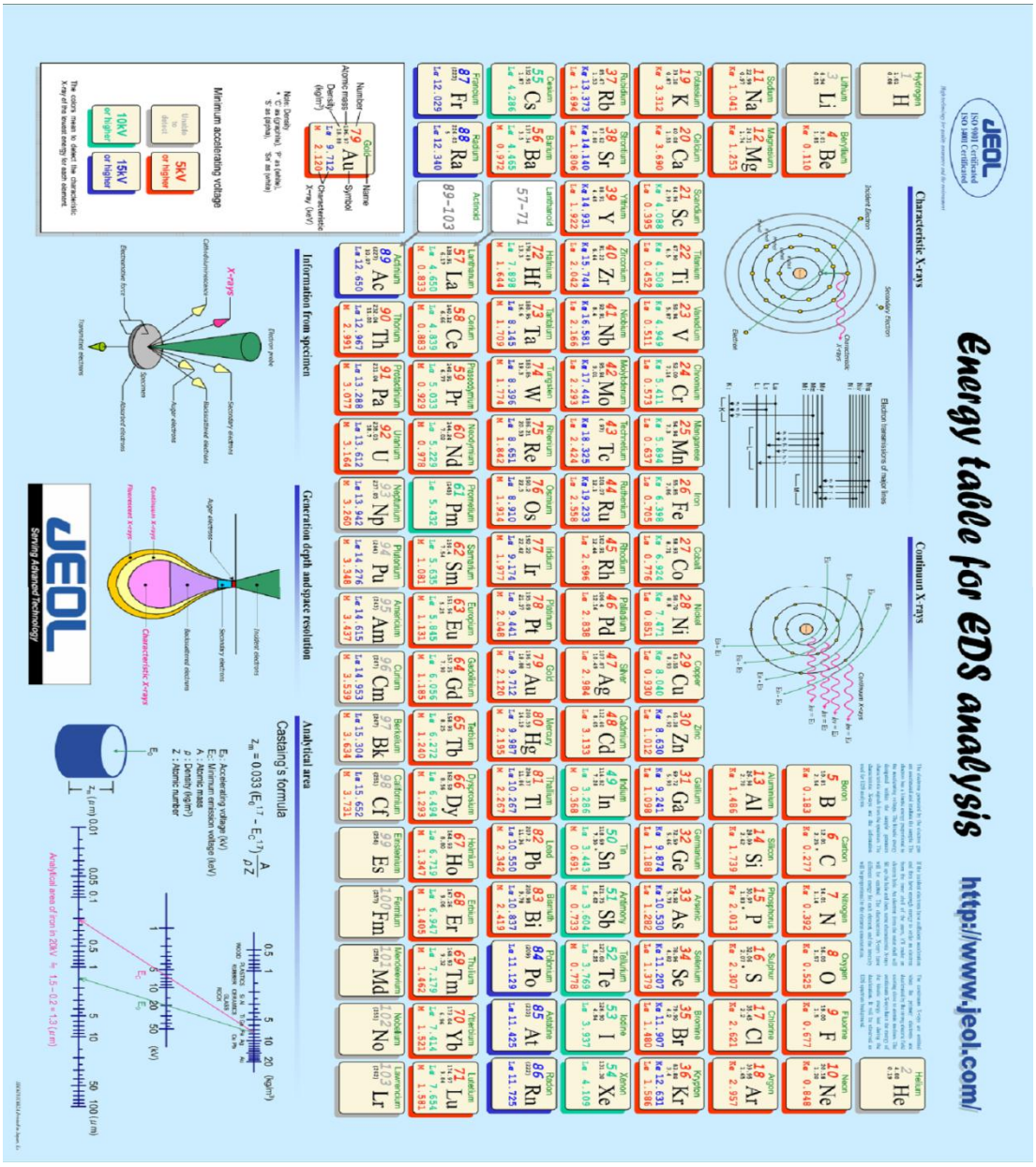

Figure A.1 Energy Table for EDS analysis

VITA

VITA

Pengyu, Zhu
Graduate School, Purdue University

Education
B.S., 2010, Shanghai University, Shanghai, China
M.S., 2015, Purdue University, West Lafayette, United States

Research Interests
Die Casting, Casting Simulation